2019-01-03

Frequency shifts and depth dependence of premotor beta band activity during percept...

Systems/Circuits

Frequency Shifts and Depth Dependence of Premotor Beta Band Activity during Perceptual Decision-Making

Chandramouli Chandrasekaran,[1,3]* Iliana E. Bray,[1]* and Krishna V. Shenoy[1,2,3,4,5,6]

[1]Department of Electrical Engineering, [2]Department of Neurobiology, [3]Howard Hughes Medical Institute, [4]Department of Bioengineering, [5]Stanford Neurosciences Institute, and [6]Bio-X Program, Stanford University, Stanford, California 94305

Neural activity in the premotor and motor cortices shows prominent structure in the beta frequency range (13–30 Hz). Currently, the behavioral relevance of this beta band activity (BBA) is debated. The underlying source of motor BBA and how it changes as a function of cortical depth are also not completely understood. Here, we addressed these unresolved questions by investigating BBA recorded using laminar electrodes in the dorsal premotor cortex of 2 male rhesus macaques performing a visual reaction time (RT) reach discrimination task. We observed robust BBA before and after the onset of the visual stimulus but not during the arm movement. While poststimulus BBA was positively correlated with RT throughout the beta frequency range, prestimulus correlation varied by frequency. Low beta frequencies (~12–20 Hz) were positively correlated with RT, and high beta frequencies (~22–30 Hz) were negatively correlated with RT. Analysis and simulations suggested that these frequency-dependent correlations could emerge due to a shift in the component frequencies of the prestimulus BBA as a function of RT, such that faster RTs are accompanied by greater power in high beta frequencies. We also observed a laminar dependence of BBA, with deeper electrodes demonstrating stronger power in low beta frequencies both prestimulus and poststimulus. The heterogeneous nature of BBA and the changing relationship between BBA and RT in different task epochs may be a sign of the differential network dynamics involved in cue expectation, decision-making, motor preparation, and movement execution.

Key words: beta band activity; decision-making; laminar; local field potential; premotor cortex; reaction time

Significance Statement

Beta band activity (BBA) has been implicated in motor tasks, in disease states, and as a potential signal for brain–machine interfaces. However, the behavioral relevance of BBA and its laminar organization in premotor cortex have not been completely elucidated. Here we addressed these unresolved issues using simultaneous recordings from multiple cortical layers of the premotor cortex of monkeys performing a decision-making task. Our key finding is that BBA is not a monolithic signal. Instead, BBA consists of at least two frequency bands. The relationship between BBA and eventual behavior, such as reaction time, also dynamically changes depending on task epoch. We also provide further evidence that BBA is laminarly organized, with greater power in deeper electrodes for low beta frequencies.

Introduction

Fluctuations in the beta (13–35 Hz) range of the local field potential (LFP) and spiking activity are consistently observed in monkeys performing instructed delay (Sanes and Donoghue, 1993; Zhang et al., 2008; Kilavik et al., 2012, 2013; Stetson and Andersen, 2014; Khanna and Carmena, 2017) and cognitive tasks (Murthy and Fetz, 1992; Lee, 2003; Rubino et al., 2006; Buschman and Miller, 2007; Pesaran et al., 2008; Feingold et al., 2015; Markowitz et al., 2015; Sherman et al., 2016; Haegens et al., 2017). Other studies demonstrated prominent beta band activity (BBA) in humans performing motor, auditory, and cognitive tasks (Saleh et al., 2010; Tzagarakis et al., 2010; Zaepffel et al., 2013; Keitel and Gross, 2016). Clinical studies suggest that BBA

Received April 22, 2018; revised Nov. 29, 2018; accepted Dec. 17, 2018.

Author contributions: C.C. and I.E.B. wrote the first draft of the paper; C.C., I.E.B., and K.V.S. edited the paper; C.C. and K.V.S. designed research; C.C. performed research; C.C., I.E.B., and K.V.S. contributed unpublished reagents/analytic tools; C.C., I.E.B., and K.V.S. analyzed data; C.C., I.E.B., and K.V.S. wrote the paper.

I.E.B. was supported by the Stanford Electrical Engineering REU Program-VPUE and a National Science Foundation Graduate Research Fellowship (Grant DGE-1656518). C.C. was supported by National Institutes of Health/National Institute of Neurological Disorders and Stroke K99 Award K99NS092972 and R00 Award 4R00NS092972-03, and supported by Howard Hughes Medical Institute as a research specialist. K.V.S. was supported by National Institutes of Health Director's Pioneer Award 8DP1HD075623, Defense Advanced Research Projects Agency Biological Technology Office NeuroFAST Award W911NF-14-2-0013, the Simons Foundation Collaboration on the Global Brain Awards 325380 and 543045, and the Howard Hughes Medical Institute.

K.V.S. is a consultant for Neuralink Corp. and is on the scientific advisory board for CTRL-Labs Inc., MIND-X Inc., Inscopix Inc., and Heal Inc. The remaining authors declare no competing financial interests. The material presented in this paper does not have any commercial relevance.

*C.C. and I.E.B. contributed equally to this work.

Correspondence should be addressed to Chandramouli Chandrasekaran at mailchand@gmail.com or mouli@stanford.edu.

https://doi.org/10.1523/JNEUROSCI.1066-18.2018

 0270-6474/19/391420-16$15.00/0

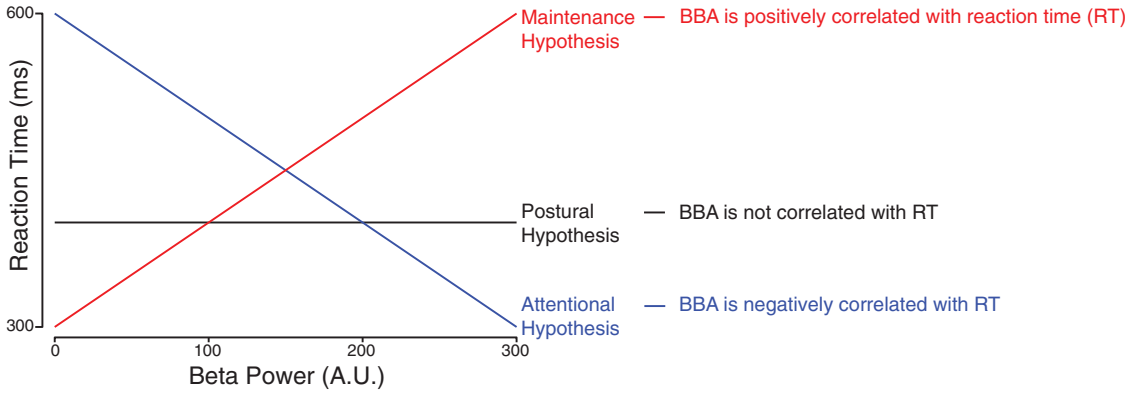

Figure 1. Three existing hypotheses about the relation between prestimulus BBA and RT. Black, horizontal line indicates the postural hypothesis of BBA, where there is no relationship between BBA and RT. Red, positively sloped line indicates the maintenance hypothesis of BBA because increased BBA would be associated with longer RTs. Blue, negatively sloped line indicates the attentional hypothesis of BBA because more BBA would signify greater attention on the task and therefore shorter RTs.

changes with age (Rossiter et al., 2014), is modulated in disease states (Brown, 2006; Brittain et al., 2014; Proudfoot et al., 2017), and may be useful for brain machine interfaces (Bai et al., 2008; Flint et al., 2013; So et al., 2014; Gilja et al., 2015; Stavisky et al., 2015; Pandarinath et al., 2017). Despite insights gained about BBA, questions about its role and origin still remain. Here, we focus on two unresolved questions.

Our primary goal is to understand the relevance of BBA in the premotor cortex for decision-making. Three hypotheses have been proposed for the role of BBA in the premotor system—postural holding, maintenance of the current state, and attention—each making specific predictions relating BBA and reaction time (RT) (Fig. 1) (Khanna and Carmena, 2015). The postural holding hypothesis posits that BBA is related to keeping the hand still during the hold period of instructed delay tasks (Baker et al., 1999; Kristeva et al., 2007; Khanna and Carmena, 2015). A second hypothesis suggests that BBA represents the desire to maintain the current state of being (e.g., resisting start of movement) (Gilbertson et al., 2005; Pogosyan et al., 2009; Engel and Fries, 2010). The attentional hypothesis emerged from the study of reach-target selection tasks and suggests that BBA reflects attention (Bouyer et al., 1987; Murthy and Fetz, 1992; Zhang et al., 2008; Saleh et al., 2010). Here, we addressed the behavioral relevance of BBA by examining the relationship between RT and BBA recorded from dorsal premotor cortex (PMd) of 2 monkeys (Zhang et al., 2008; Saleh et al., 2010; Tzagarakis et al., 2010; Kilavik et al., 2012; Khanna and Carmena, 2017). The monkeys performed an attentionally demanding visual reach decision-making task that involved the somatomotor system and induced significant variation in RT beyond the variability induced by the different stimulus difficulties.

Our secondary goal is to further elucidate the laminar organization of BBA in premotor cortex. Some studies suggest that deeper cortical layers of motor cortex and other brain areas are involved in the generation of BBA (Wetmore and Baker, 2004; Chen and Fetz, 2005; Roopun et al., 2006; Yamawaki et al., 2008; Bastos et al., 2018). Others suggest that all cortical layers in motor cortex are involved in BBA (Kondabolu et al., 2016; Sherman et al., 2016). Identifying how BBA changes as a function of cortical depth could facilitate the development of the next generation of computational models (Kopell et al., 2011; Lee et al., 2013; Bhatt et al., 2016; Sherman et al., 2016). To study the laminar organization of BBA, we used multicontact electrodes that provided simultaneous recordings across different cortical depths.

We observed that both prestimulus and poststimulus BBA was correlated to RT, thus ruling out the postural holding hypothesis. Poststimulus BBA was positively correlated with RT throughout the beta range, while the correlation between RT and prestimulus BBA was positive in the low beta frequencies (~13–20 Hz) and negative in the high beta frequencies (~25–35 Hz). This frequency-dependent correlation between RT and prestimulus LFP power spectra likely emerges from a shift in prestimulus BBA to higher frequencies for faster RTs. We also found that deeper electrodes demonstrated more low beta power both prestimulus and poststimulus.

Materials and Methods

Experimental design

Here we provide a brief description of the experimental design. Additional details about training, surgery, and a description of single-neuron responses during the various epochs are found in a previous study (Chandrasekaran et al., 2017). This study focuses on analysis of the prestimulus (600 ms period before the onset of the checkerboard stimulus) and poststimulus (300 ms period after the onset of the checkerboard stimulus) LFP recorded during the same experiments. We also briefly examine the 300 ms period after movement initiation, which we term movement period.

Subjects. Our experiments were conducted using 2 adult male macaque monkeys (Macaca mulatta; Monkey T, 7 years, 14 kg; Monkey O, 11 years, 15.5 kg) trained to reach for visual targets for a juice reward. Monkeys were housed in a social vivarium with a normal day/night cycle. The protocols for our experiments were approved by the Stanford University Institutional Animal Care and Use Committee. We initially trained monkeys to come out of the cage and sit comfortably in a chair. After initial training, we performed sterile surgeries during which monkeys were implanted with head restraint holders (Crist Instruments, cylindrical head holder) and standard recording cylinders (Crist Instruments). Cylinders were centered over caudal PMd (+16, 15 stereotaxic coordinates) and placed surface normal to the cortex. We covered the skull within the cylinder with a thin layer of dental acrylic/palacos.

Apparatus. The general setup for the experiments is shown in Figure 2*a*. Monkeys sat in a customized chair (Crist Instruments, Snyder Chair) with the head restrained via the surgical implant. The arm not used for reaching was gently restrained using a tube and a cloth sling. Experiments were controlled and data collected under a custom computer control system (xPC target and Psychophysics Toolbox). Stimuli were displayed on an Acer HN2741 computer screen placed ~30 cm from the monkey. A photodetector (Thorlabs PD360A) was used to record the onset of the visual stimulus at a 1 ms resolution. Each session we taped a small reflective hemispheral bead (11.5 mm, NDI Digital passive spheres) to the middle digit of the right hand (left hand for Monkey O). The bead was

taped 1 cm from the tips of the fingers, and the position of this bead was tracked optically in the infrared (60 Hz, 0.35 mm root mean square accuracy; Polaris system; Northern Digital). Eye position was tracked with an overhead infrared camera (estimated accuracy of 1°, Iscan). To get a stable eye image for the overhead infrared camera which acquires the eye image, an infrared mirror transparent to visible light was positioned at a 45° angle (facing upwards) immediately in front of the nose. This mirror reflected the image of the eye in the infrared range while letting visible light pass through. A visor placed around the chair prevented the monkey from bringing the bead to his mouth or touching the infrared mirror or the juice tube.

Task structure. Experiments consisted of a sequence of trials, which each lasted a few seconds; successful trials resulted in a juice reward, and unsuccessful trials resulted in a time-out lasting 2–4 s. An example trial timeline is shown in Figure 2*b*. Monkeys used their unrestrained arm (Monkey T used his right arm, Monkey O used his left arm) to reach to touch either red or green targets based on the dominant color in a central, static checkerboard cue composed of isoluminant red and green squares. For every trial, the monkey placed his unrestrained arm on a central target (diameter = 24 mm) and fixated on a small white cross (diameter = 6 mm). After ~350–400 ms had elapsed, two isoluminant colored targets appeared 100 mm to the right and left of the central target. The target configuration was randomized so that colors were not always tied to reach directions: sometimes the red target was on the left and green on the right, whereas other trials had the opposite configuration. After an additional hold period (varying from 400 to 900 ms), a static checkerboard cue (15 × 15 grid of squares; each square 2.5 mm × 2.5 mm) composed of isoluminant red and green squares appeared on the screen around the fixation cross (example stimuli are shown in Fig. 2*c*). The monkeys reached for the target whose color matched the dominant color in the central checkerboard cue. For example, when there was more green than red in the central checkerboard cue, the monkey had to choose the green target. To "choose" a target, the animals moved their hand from the central hold point and stably held a target for a short duration (minimum of 200 ms).

The task was an RT paradigm, so the monkeys were free to initiate their reach whenever they felt there was sufficient evidence for them to provide a response. We did not impose any delayed feedback procedure in this task, such as a delay between the time of reward and the completion of a reach for a correct target (Roitman and Shadlen, 2002). The juice reward was provided to the monkey immediately after the monkey provided a correct response.

We parameterized the checkerboard cue at several different levels from almost fully red to almost fully green. We used 14 levels of red (ranging from 11 red squares to 214 red squares) in the central checkerboard cue. Each level of red had a complementary green level (e.g., 214 R, 11 G; and 214 G, 11 R squares). This defined seven levels of unsigned color coherence (defined as $C = \frac{100 \times |R - G|}{R + G}$), ranging from 4–90%. The corresponding signed color coherence was estimated without taking the absolute value of the difference $\left(SC = \frac{100 \times (R - G)}{R + G} \right)$.

For Monkey T, we used a uniform distribution of hold period durations between the onset of the targets and the onset of the checkerboard cue. Monkey O attempted to anticipate the checkerboard cue onset. To minimize this anticipation and reduce predictability, we used an exponential hold period duration (400–800 ms) between the onset of the targets and the onset of the checkerboard cue.

Electrophysiological recordings. Stereotactic coordinates, known response properties of PMd and motor cortex, and neural responses to muscle palpation served as our guides for electrophysiological recordings. We placed the chamber's surface normal to the cortex to align with the skull of the monkey, and recordings were performed perpendicular to the surface of the brain. Recordings were made anterior to the central sulcus, lateral to the spur of the arcuate sulcus, and lateral to the precentral dimple. For both monkeys, we confirmed our estimate of the upper and lower arm representation by repeated palpation at a large number of sites to identify muscle groups associated with the sites. Monkey T used his right arm to perform tasks, whereas Monkey O used his left arm. Recordings for this study were performed in PMd contralateral to the arm used by the monkey. We focused on PMd due to its known role and greater neural activity during the preparatory and premovement period, as well its established role in decision-making (Thura and Cisek, 2014; Coallier et al., 2015; Chandrasekaran et al., 2017).

We performed linear multicontact electrode (U probe) recordings in the same manner as single-electrode recordings with some minor modifications. We used a slightly sharpened guide tube to allow the U probe to penetrate the dura more easily. We also periodically scraped away any overlying tissue on the dura under anesthesia. Sharp guide tubes and scraping away dura greatly facilitated penetration of the U probe. We typically penetrated the brain at very slow rates (~2–5 μm/s). Once we felt that we had a reasonable sample population of neurons potentially spanning different cortical layers, we stopped and waited for 45–60 min for the neuronal responses to stabilize. The experiments then progressed as usual. We used 180-μm-thick, 16-electrode U probes with an interelectrode spacing of 150 μm; electrode contacts were ~100 kΩ in impedance. Signals were referenced to a single common reference (a guide tube in contact with saline in the chamber).

We attempted to minimize the variability in U probe placement on a session-by-session basis so that we could average across sessions. Our approach was to place the U probe so that the most superficial electrodes (electrodes 1, 2 on the 16-channel probe) were able to record multiunit spiking activity. Any further withdrawal of the electrode from the cortex resulted in the spiking activity for those electrodes disappearing and a change in the overall activity pattern of the electrode (suppression of overall LFP amplitudes). Similarly, driving the electrodes deeper resulted in multiphasic extracellular waveforms and also a change in auditory markers, which were characterized by decreases in overall signal intensity and frequency content; both markers suggested that the electrode entered white matter (Cooper et al., 1969). We used these physiological markers as a guide to place electrodes and thereby minimize variability in electrode placement on a session-by-session basis. Recording yields and this careful electrode placement were in general better in Monkey T (average of ~16 units per session) than Monkey O (average of ~9 units per session).

The insertion technique necessitated a careful watch over the electrode while lowering to ensure that it did not bend, break at the tip, or excessively dimple the dura. We therefore were unable to use a grid system to precisely localize the location of the U probes on different days and to provide a map of how laminar profiles change in the rostrocaudal direction.

LFPs. LFP recordings in Monkey T were performed using a 2 kHz sampled signal. We then resampled this signal at 1 kHz and performed subsequent spectral analysis on appropriate time epochs. For Monkey O, two methods were used. For 17 of the sessions, we recorded LFP at 2 kHz, as in Monkey T. For the remaining sessions, we recorded broadband extracellular activity at 30 kHz. We resampled this broadband extracellular signal at 1 kHz and then again used it for subsequent spectral analysis. All resampling was performed using the MATLAB resample command that first applies a delay compensating low pass filter and then subsequently resamples the data avoiding aliasing.

RT. RT is defined as the time between stimulus onset and the time at which the monkey moved his hand from the central holding location and began moving the hand toward one of the targets. RT was estimated using a velocity thresholding method (Chandrasekaran et al. 2017).

The RT by definition does not include the movement time, which is time the hand is moving. RT is described in units of milliseconds. An RT ≤300 ms indicates that the monkey most likely did not incorporate the presented stimulus into his response. These trials are not representative of decision-making based on the provided stimulus and were therefore removed from our analysis.

Statistical analysis

Psychometric curves for accuracy. For the analysis of the behavior, we used the same 24 sessions for Monkey T (47,483 trials) and 44 sessions for Monkey O (70,250 trials) from which we examined electrophysiological data. Fits to psychometric curves and RT regressions were performed on a per-session basis and then averaged over sessions. The behavior of an

average session was estimated from ~1500 trials. RT was estimated for each session by including both correct and incorrect trials for each signed color coherence.

We fit psychometric curves that describe how discrimination accuracy changed as a function of unsigned color coherence. For every experiment, we estimated the monkey's sensitivity to the checkerboard cue by estimating the probability (p) of a correct choice as a function of the unsigned color coherence of the checkerboard cue (C). We used the psignifit toolbox to fit this accuracy function using a Weibull cumulative distribution function (Wichmann and Hill, 2001) as follows:

$$p(c) = 1 - 0.5e^{(-(c/\alpha)^{\gamma})}$$

The discrimination threshold, α, is the color coherence level at which the monkey would make 81.6% correct choices. The second parameter, γ, describes the slope of the curve. The mean α parameter across sessions was used as the threshold. We fit threshold and slope parameters on a session-by-session basis and averaged the estimates. The mean and SD of the threshold estimates are reported in Figure 2*d*.

RT versus coherence. To examine whether RT changed with color coherence, we adopted the procedure from Roitman and Shadlen (2002) and used a linear regression between mean RT and log unsigned coherence (4%–90%).

$$RT(c) = intercept + a_c\, log_e(c)$$

We fit this regression model (see Fig. 2*e*) with a_c as the slope of the regression and report this number in the text.

LFP filtering. We removed the DC offset from the LFP time series and used a second-order IIR notch filter to remove line noise (Mitra and Bokil, 2008; Mitra et al., 2017). Line noise, which is centered at 60 Hz, arises from radiative electrical pickup from lights and electrical equipment. We centered the filter at 60 Hz and set the quality factor (related to the filter bandwidth) to 35.

Multitaper power spectra. To estimate the power spectra in Figures 3, 4, 5, 6, 8, we used the Chronux toolbox for MATLAB (Mitra and Bokil, 2008; Mitra et al., 2017), which implements the multitaper spectral estimation method, with a time-bandwidth product of three and with five leading tapers. Choice of other tapers did not result in any changes in our conclusions. The power spectra have arbitrary units (A.U.) before they are normalized.

Normalization of power spectra. We normalized the power spectra over all power values (including all frequencies) from all trials for a given electrode in a given session. We calculated the z score by subtracting the mean (of all power values from all trials in that session) from each point and dividing by the SD across trials.

SE. SE was defined as $s/\sqrt{n}$, where s is the SD of the power spectra for several sessions with respect to the sessions, and n is the number of sessions. SE is shown in shading in plots of power spectra.

Split into RT quantiles. We first calculated the breaks for the RT percentiles for that monkey on that session, separating the trials with RTs either >85% of trials in that session and the trials with RTs <15% of trials in that session.

Correlation between BBA and RT. For each electrode, per session of data, we computed the partial Spearman correlation between the normalized power at each frequency with RT, controlling for the coherence of the checkerboard. Correlations were computed over large numbers of trials for each electrode (mean of 1265 trials per electrode).

We used a partial correlation to control for the confounding variable, the coherence of the checkerboard, which we know affects the RT and will affect the postcue LFP power spectra and would therefore have otherwise given misleading correlation values.

False discovery rate (FDR) adjustment. Significance of the correlation values was adjusted using the Benjamini and Hochberg (1995) procedure for controlling the FDR of a family of hypothesis tests (Groppe, 2015).

Combining across animals. We combined animals when they showed the same trends. Whenever data are shown combined across animals, it was first normalized (as explained above); then sessions from each animal were pooled, and the average across all these sessions was calculated. If statistical tests were done, they were done across the full pooled set of sessions.

Simulating relationships between BBA and RT. To clarify the mathematical relationship between BBA and RT, we performed a series of simulations (see Fig. 6). We first randomly generated an RT value within the range typically observed for our monkeys. Then, we created a variety of LFP signals in which the frequency and amplitude were either constant or related in some way to the RT that was generated. The relationship between frequency, amplitude, and RT is specified in the equations below, where randn signifies a random number drawn from the normal distribution. Within each frequency and amplitude relationship, we generated 1000 RTs and corresponding LFP signals. We then calculated the power spectrum for each simulated LFP signal before correlating the power spectra to the randomly generated RT. Each frequency and amplitude relationship resulted in a different correlation with RT. The equations below match the panels shown in Figure 6.

$$\begin{aligned} \text{Frequency} &= 28 + 1.2 * \text{randn} \\ \text{Amplitude} &= .3 + 5\text{e-}6 * \text{RT} + .001 * \text{randn} \end{aligned} \quad \text{(i)}$$

$$\begin{aligned} \text{Frequency} &= 28 + 1.2 * \text{randn} \\ \text{Amplitude} &= .3 - 5\text{e-}6 * \text{RT} + .001 * \text{randn} \end{aligned} \quad \text{(ii)}$$

$$\begin{aligned} \text{Frequency} &= 28 + 1.2 * \text{randn} + .003 * \text{RT} \\ \text{Amplitude} &= 1 + .04 * \text{randn} \end{aligned} \quad \text{(iii)}$$

$$\begin{aligned} \text{Frequency} &= 28 + 1.2 * \text{randn} - 0.003 * \text{RT} \\ \text{Amplitude} &= 1 + .04 * \text{randn} \end{aligned} \quad \text{(iv)}$$

$$\begin{aligned} \text{Frequency} &= 28 + 1.2 * \text{randn} - .003 * \text{RT} \\ \text{Amplitude} &= .3 + 5\text{e-}6 * \text{RT} + .001 * \text{randn} \end{aligned} \quad \text{(v)}$$

$$\begin{aligned} \text{Frequency} &= 28 + 1.2 * \text{randn} - .003 * \text{RT} \\ \text{Amplitude} &= .3 - 5\text{e-}6 * \text{RT} + .001 * \text{randn} \end{aligned} \quad \text{(vi)}$$

Wavelet analysis. We created time–frequency representations of our data using the wavelet analysis implemented in the EEG toolbox from the Computational Memory Lab of University of Pennsylvania (2008). We used Morlet wavelets, which are standard for analysis of electroencephalographic signals and LFPs (Tallon-Baudry et al., 1997; Lakatos et al., 2007; Ghazanfar et al., 2008; Chandrasekaran and Ghazanfar, 2009). An excellent primer on the use of wavelets to analyze electrophysiological signals is available in Tallon-Baudry et al. (1997).

A key parameter that needs to be chosen in the wavelet analysis is the ratio between the central frequency and the SD in the frequency domain (f_0/σ_f). This parameter in turn leads to a balance between time and frequency resolution, with the SD in the frequency domain given as $\sigma_t = 1/(2\pi\sigma_f)$. We use a wavelet parameter of 6, which is very similar to wavelet parameters used in previous studies (Tallon-Baudry et al., 1997; Lakatos et al., 2007; Ghazanfar et al., 2008). At 24 Hz, a typical beta band frequency, and a wavelet parameter of 6, our frequency resolution would be 4 Hz, and the time resolution would be ~39 ms. We chose center frequencies (f_0) according to the equation $f_0 = 2^x$, where $x = 0.5{:}0.1{:}7$, which gave us frequencies from 1.42 to 128 Hz.

Results

Two trained monkeys (Monkeys T and O) discriminated the dominant color of a central, static checkerboard cue composed of mixtures of red and green squares and used an arm movement to report the decision (Fig. 2*a*) (Coallier et al., 2015). Figure 2*b* depicts a trial timeline. The trial began when the monkey touched the center target and fixated on the cross. After a variable target viewing period, the red-green checkerboard cue appeared. The task of the monkey was to make an arm movement toward the target (red vs green) that matched the dominant color of the

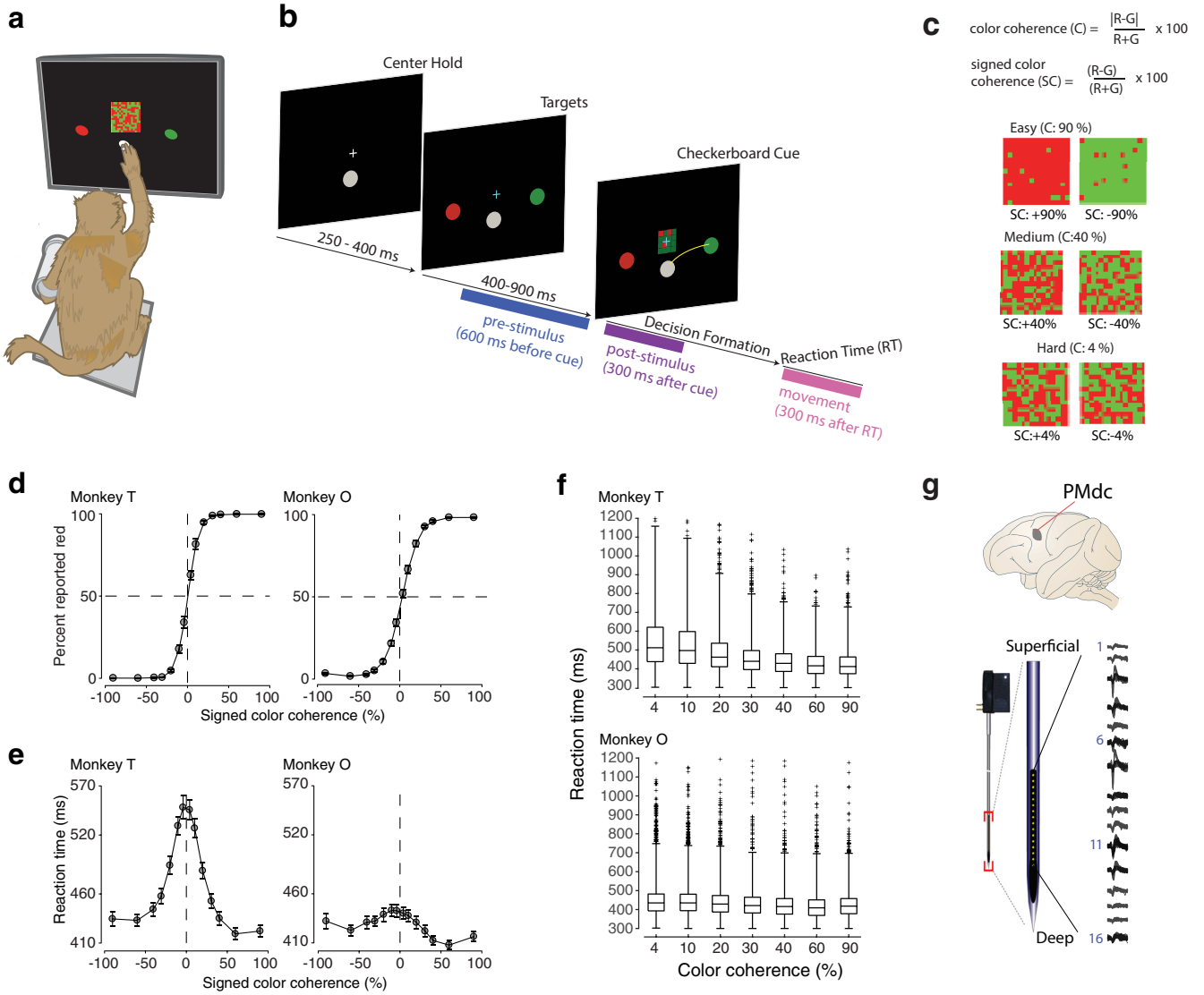

Figure 2. Recording locations, techniques, task, and discrimination behavior. ***a***, An illustration of the experimental setup for data gathering in the discrimination task. We gently restrained the resting arm with a plastic tube and cloth sling. We tracked a reflective IR bead taped on the middle digit of the unrestrained hand to mimic a touch screen and to provide an estimate of instantaneous arm position. We tracked eye position using an infrared reflective mirror placed in front of the monkey's nose. ***b***, Timeline of the discrimination task, showing the prestimulus period (the 600 ms period before checkerboard onset, depicted as a blue rectangle), poststimulus period (the 300 ms period after checkerboard onset depicted in purple), and postmovement period (the 300 ms period after movement initiation at the RT shown in pink). ***c***, Examples of different stimulus ambiguities used in the experiment parameterized by the color coherence of the checkerboard defined as follows: $C = \frac{100 \times |R - G|}{R + G}$. The corresponding signed color coherence is defined as follows: $SC = \frac{100 \times (R - G)}{R + G}$. Positive values of signed color coherence indicate more red than green squares and vice versa. ***d–e***, Average discrimination performance (***d***) and RT (***e***) over sessions of the 2 monkeys as a function of the signed color coherence of the checkerboard. RT plotted here includes both correct and incorrect trials for each session and then averaged across sessions. Gray markers represent measured data points along with 2x (SE) estimated over sessions, although variation is so small that they are difficult to see in ***d***. The black line segments are drawn in between these measured data points to guide the eye. For most data points in ***d***, the error bars lie within the markers. ***d***, ***e***, *x* axes represent the signed color coherence in %. *y* axes represent the percentage responded red in ***d*** and RT in ***e***. Also shown in ***d*** are discrimination thresholds (mean ± SD over sessions) estimated from a Weibull fit to the overall percentage correct as a function of unsigned coherence. The discrimination threshold is the color coherence level at which the monkey made 81.6% correct choices. A total of 24 sessions for Monkey T (47,483 trials) and 44 sessions for Monkey O (70,250 trials) went into these averages. ***f***, Box-and-whisker plot of RT as a function of unsigned checkerboard coherence. For each coherence, the central mark of the box indicates the median, the bottom and top edges of the box reflect the 25th and 75th percentiles, respectively, the maximum whisker length is specified as three times the interquartile range, and outliers are plotted as plus symbols. There is large variation of RTs both across and within coherences. ***g***, Location of PMd along with an example recording from a 16-electrode, 150 μm spacing U probe. The neuronal waveforms are taken from the recordings, and properties of these neuronal responses were reported in a previous study.

checkerboard cue. We term the time period (600 ms) before the checkerboard cue appeared as the prestimulus period, the period (300 ms) after the checkerboard cue appeared as the poststimulus period, and the time period (300 ms) after movement initiation when the movement is performed as the movement period.

We parameterized difficulty of the discrimination (example stimuli shown in Fig. 2*c*) by an unsigned color coherence measure (C) defined as the absolute difference in the number of red and green squares normalized by the total number of squares in the checkerboard ($C = 100 * |R - G|/(R + G)$). A corresponding signed color coherence measure (SC) is defined as $SC = 100 * (R - G)/(R + G)$. We previously reported the behavior of the monkeys while they performed this task (Chandrasekaran et al., 2017). Here we present the psycho-

metric and chronometric curves for the sessions where we examined the LFP.

On average across sessions, more ambiguous checkerboards resulted in more errors (Fig. 2*d*). We fit the proportion correct as a function of unsigned coherence (C) using a Weibull function to estimate slopes and psychometric thresholds (average R^2; Monkey T: 0.99, over 24 sessions, 47,483 trials; Monkey O: 0.99 over 44 sessions, 70,250 trials; slope (β), mean ± SD over sessions, Monkey T: 1.30 ± 0.16; Monkey O: 1.26 ± 0.15). Monkey T displayed more sensitivity than Monkey O (thresholds are computed on a per-session basis and averaged over sessions at 81.6% correct, mean ± SD: Monkey T, 9.87 ± 1.12%; Monkey O: 15.05 ± 1.79%, two-tailed test, Wilcoxon rank sum comparing median thresholds, $p = 1.29\text{e-}11$).

More ambiguous checkerboards also resulted in a slower mean RT (Fig. 2*e*). We tested whether mean RT increased as $\log_e$ unsigned coherence decreases (that is harder stimulus difficulties), as in Roitman and Shadlen (2002); average R^2, Monkey T: 0.94; Monkey O: 0.59; slope of regression: mean ± SD over sessions, Monkey T: −41.1 ± 6.3 ms/$\log_e$ unsigned coherence (%); Monkey O: −8.6 ± 4.5 ms/$\log_e$ unsigned coherence (%). Monkey T had a larger range of RTs compared with Monkey O (comparing the RT range between easiest and hardest difficulties estimated over sessions; Monkey T: 115 ± 19 ms; Monkey O: 28 ± 11 ms, Wilcoxon rank sum comparing median ranges of RT, $p = 1.29 \times 10^{-11}$).

Although color coherence explains considerable variation in RT, there is significant variation in RT that is not explained by the coherence. A trial-by-trial linear regression between RT and unsigned stimulus coherence only explained 10.8% of the variance in Monkey T and only 1.3% in Monkey O. This variation in RT is readily apparent even within a given color coherence (boxplot shown in Fig. 2*f*), and our hypothesis is that this RT variability is at least in part related to fluctuations in BBA (Fig. 1) (Pogosyan et al., 2009; Kilavik et al., 2012; Chandrasekaran et al., 2017; Khanna and Carmena, 2017).

LFP and neuronal responses during the prestimulus period show prominent BBA

We first examined the LFPs recorded in PMd, specifically examining how the power across different frequencies of the LFP changed throughout the reach decision task. BBA is apparent in the prestimulus period (600 ms before the appearance of the checkerboard stimulus), decreases during the poststimulus decision-formation period, and remains low during the movement epoch (Fig. 3*a*,*b*). This prestimulus increase in power in the 15–35 Hz range is consistent with the definition of BBA in both frequency (15–35 Hz) and timing within task behavior (Sanes and Donoghue, 1993; Baker et al., 1997; Kilner et al., 1999; Riddle and Baker, 2006; Rubino et al., 2006; Baker, 2007; Klostermann et al., 2007; Chakarov et al., 2009; Zaepffel et al., 2013). Decreases in BBA after movement onset are also consistent with these and other prior reports of beta event related desynchronization. Finally, activity in the δ band (0.5–4 Hz), θ band (4–7 Hz), and α band (8–12 Hz) are present both before and after checkerboard onset (Fig. 3*a*).

Several other analyses confirmed the existence of BBA during the prestimulus period. Temporal fluctuations in the beta band were readily visible in individual trials of the LFP, suggesting that we are not artificially separating a broadband signal into oscillations in a specific frequency band (Fig. 3*c*). The power spectra for the trials shown in Figure 3*c* corroborated this observation of signals in the 15–35 Hz range (Fig. 3*d*). We examined the average power spectrum over all trials, electrodes, and sessions for three different task periods: prestimulus, poststimulus, and movement (Fig. 3*e*). Significant BBA was consistently observed in our population recording during the prestimulus period with a peak frequency approx 25 Hz.

LFP from the poststimulus period shows activity in both the beta and γ bands

Across both monkeys, BBA observed in the poststimulus period, which is the 300 ms period after the onset of the checkerboard, differs from prestimulus BBA (Fig. 3*e*). After stimulus onset, BBA has decreased peak power and a broader peak (covering more frequencies). The frequencies present are, however, still consistent with the broad frequency definition of BBA. The power spectra in Figure 3*e* also suggest that activity in the γ band was higher in the poststimulus compared with the prestimulus period.

To better understand the changes between the periods, we normalized the power in the poststimulus period by the prestimulus period (Fig. 3*f*; power spectrum $= \frac{post\ stimulus - pre\ stimulus}{pre\ stimulus}$). This normalization suggested a decrease in BBA, an increase in low-frequency (δ and θ) activity, and an increase in low γ activity from the prestimulus to poststimulus epoch.

RT covaries with prestimulus BBA frequency and power

Our first goal in this study was to better understand the relationship between BBA from the prestimulus and poststimulus periods and behavior, keeping in mind the various hypotheses about BBA. First, we examined whether there were significant relationships between the properties of prestimulus BBA and RT.

As an initial, exploratory analysis, we examined the extremes of the data by splitting the data based on RT alone (including all the checkerboard coherences) into the fastest trials with the smallest 15% of RTs and the slowest trials with the largest 15% of RTs and compared the average power spectra of the two groups for each monkey. Using the fifth and 95th percentiles suggested similar patterns. Across both monkeys during the prestimulus period, this analysis suggested that the faster RTs have more power in the higher frequencies of BBA (~25–30 Hz) (Fig. 4*a*,*b*). In Monkey T, the slower RT trials have slightly more power in the lower frequencies of BBA (~15–25 Hz). In Monkey O, the faster (smallest) RTs have more power for both the low and high frequencies of BBA. This initial exploratory analysis suggests that the frequency and power of BBA covary with RT.

To more rigorously quantify this relationship between RT and the properties of prestimulus BBA, we performed three different analyses, which we detail below.

First, we tested whether the two RT groupings had significantly different peak frequencies. For each electrode and each trial, we identified the peak frequency within the beta band (ignoring the strong δ, θ, and α activity) for the prestimulus period. Within each RT-based group (one for the 15% slowest and one for the 15% fastest RTs), we averaged peak frequency over trials and then electrodes, finally pooling the sessions across monkeys. We tested the distributions of peak frequencies during the prestimulus period and found they were statistically different for the two RT groups (two-sided sign test, 0.57 Hz higher median peak frequency for the faster RT trials, $p = 0.001$). Results were similar when using the fifth and 95th percentiles.

Second, we examined the correlation between the peak frequency and RT. We performed this analysis using partial Spearman correlations (i.e., we estimated the correlation between the

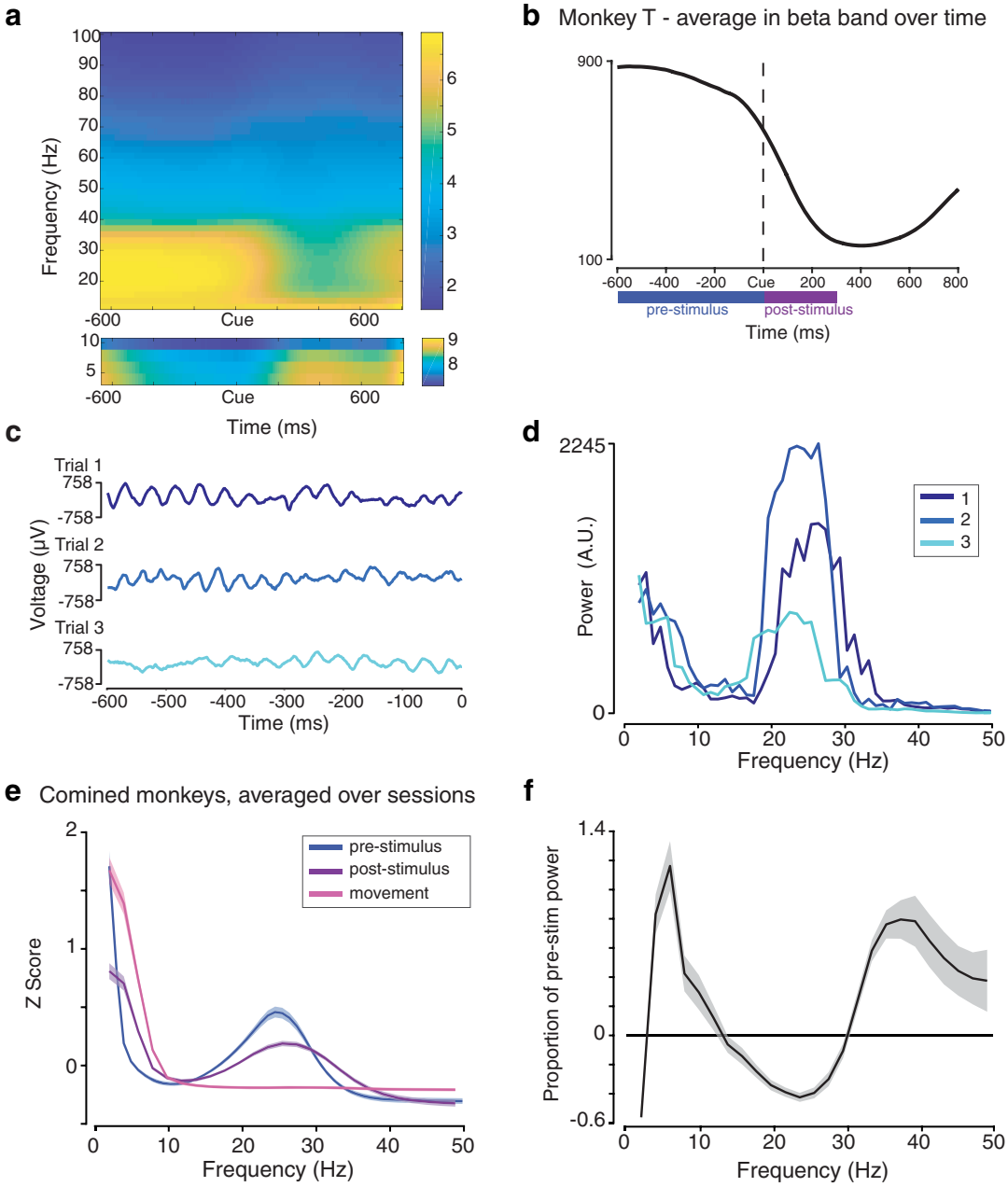

Figure 3. Existence of BBA during hold period before the visual stimulus. ***a***, Multitaper spectrogram aligned to checkerboard onset (indicated with Cue), averaged over all electrodes, trials, and sessions for Monkey T. The *y* axis represents frequency and is shown in Hertz. The *x* axis represents time in milliseconds. Color represents natural log power in log of arbitrary units. The spectrogram has been split to show the range of activity for low frequencies <10 Hz and higher frequencies from 10 to 100 Hz. Clear presence of prestimulus BBA is seen, with lower-power poststimulus BBA. ***b***, Activity in the beta band (13–30 Hz) over time, averaged over all electrodes, trials, and sessions for Monkey T. The *y* axis represents power in (A.U.). The *x* axis represents time in milliseconds. ***c***, The LFP time series of three trials of Electrode 2 during a single session. The colors are unique to each trial and consistent with subplot (***d***). The time series are shown as microvolts per millisecond. ***d***, Power spectra of three example trials during the epoch before the checkerboard. Power in (A.U.) is plotted against frequency (Hertz). ***e***, Normalized power spectra of the LFP during the epoch before the checkerboard (blue), after the checkerboard (purple), and after movement (pink). Data were separately averaged for each monkey over trials and then electrodes. Next, data were combined for the 2 monkeys and were averaged over sessions. The power spectra were normalized, and their *z* scores are plotted against frequency (Hertz). Shaded regions represent SE over sessions. ***f***, A baseline correction of power per frequency for the poststimulus period. The power spectrum proportional change calculated as $\frac{post\ stimulus - pre\ stimulus}{pre\ stimulus}$. Shading represents SE over sessions. The poststimulus and prestimulus power spectra used have not been normalized and have been averaged over trials, then over electrodes, and last over pooled monkeys' sessions.

peak frequency and RT while using checkerboard coherence as a covariate). We averaged this correlation over electrodes for each session, pooled both monkeys' sessions, and then performed a sign test for significance of the correlation relative to 0. We found that faster RTs were accompanied by higher prestimulus beta band peak frequency, as seen from the negative correlations between these two variables (median r across sessions $= -0.05$, $p = 5.22 \times 10^{-4}$).

Third, we examined whether the relationship between RT and power was consistent with our hypotheses about BBA from Figure 1. Figure 4*c* shows the Spearman correlation between RT and power for each frequency for a single session from Monkey T. For

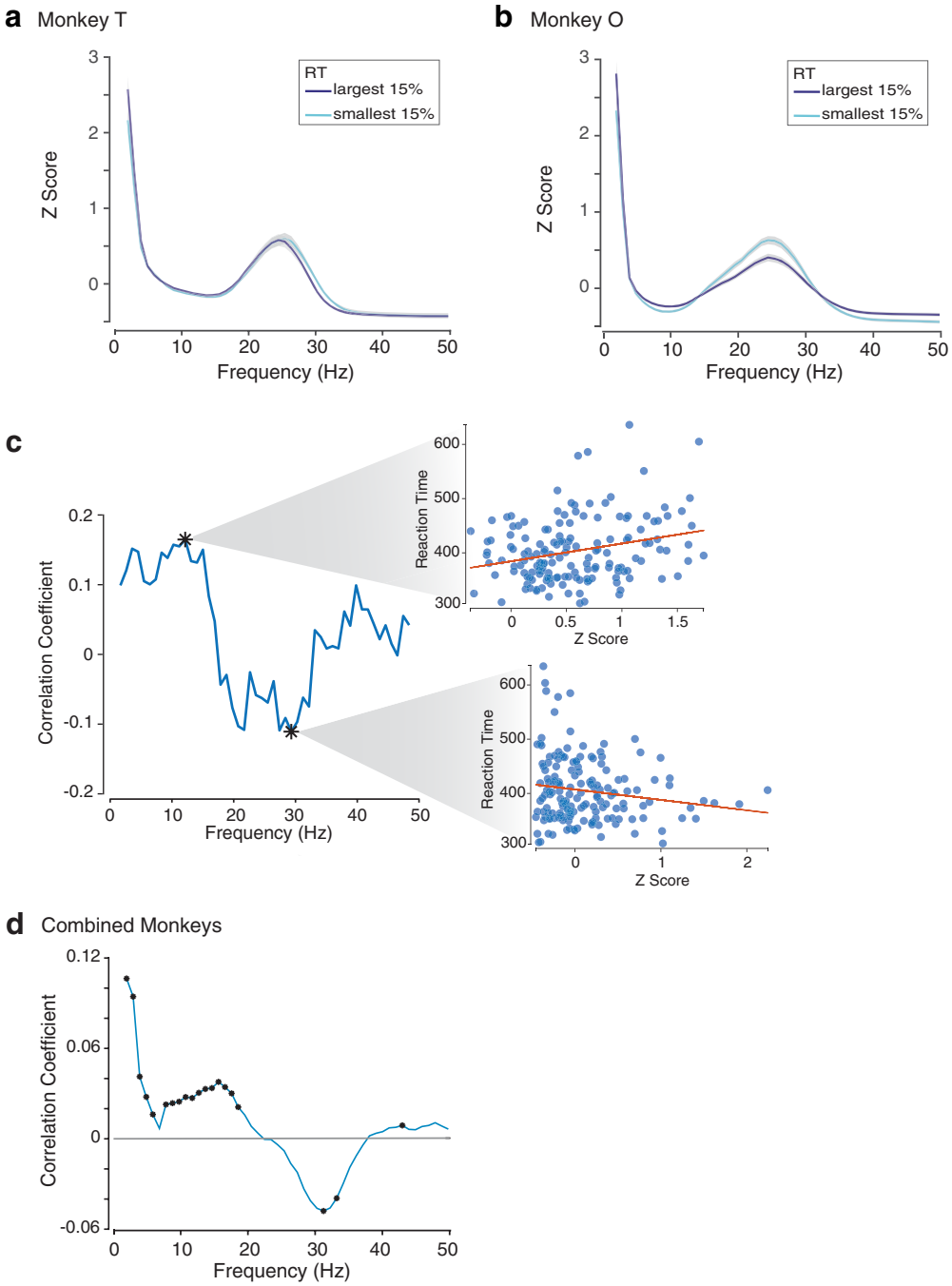

Figure 4. Relation between prestimulus BBA and RT. ***a***, ***b***, Normalized prestimulus power spectra grouped into two RT quantiles and averaged over all trials within that group, all electrodes, and all sessions for Monkey T (***a***) and Monkey O (***b***). The two quantiles are the 15% largest (slowest) RTs and the 15% smallest (fastest) RTs. The power spectra have been normalized, and their *z* scores are plotted against frequency (Hertz). Gray represents SE over sessions. ***c***, The partial correlation between RT and normalized power at each frequency, averaged over electrodes, for all trials with the easiest checkerboard coherence within one session. At the peaks in correlation, a scatter plot of RT versus normalized power (averaged over electrodes) at that frequency is shown. Orange line represents RT regressed as a function of an intercept and normalized power at that frequency. ***d***, Partial correlation between normalized prestimulus power spectra with RT as a function of frequency. Data were separately averaged for each monkey over trials and then electrodes. Next, data were combined for the 2 monkeys and were averaged over sessions. *Points along the curve where the correlation is significant (adjusted p value <0.05).

this analysis, we selected all trials with the easiest checkerboard coherence and then calculated the correlation between RT and the normalized power at each frequency for these trials. We then averaged over electrodes (Fig. 4*c*). The correlation was positive for the low beta band (peak at 12.69 Hz with $r = 0.17$). The inset shows a scatter plot of RT versus normalized power (averaged over electrodes) at that frequency for each trial. A regression between RT as a function of an intercept and normalized power (after excluding outlier trials) at 12.69 Hz was significant (beta = 32.73, $t_{(155)} = 3.42$, $p = 8.04 \times 10^{-4}$), consistent with the maintenance hypothesis. At higher beta frequencies, the relationship between BBA and RT was negative (at 30.27 Hz, $r = -0.11$). At this frequency, a regression of RT as a function of an intercept and normalized power was negative and significant (beta = −19.33, $t_{(161)} = -2.02$, $p = 0.045$), consistent with the attentional hypothesis.

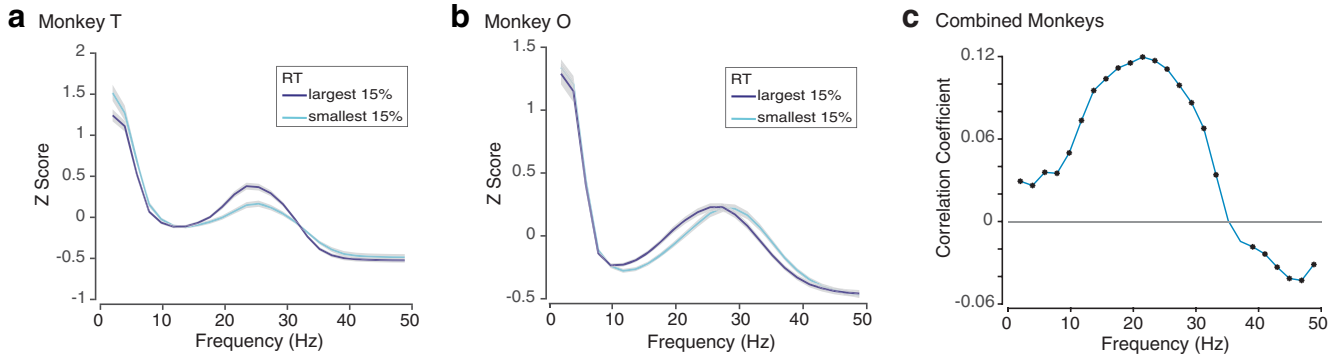

Figure 5. Relation between poststimulus BBA and RT. ***a***, ***b***, Normalized poststimulus power spectra grouped into two RT quantiles and averaged over all trials within that group, all electrodes, and all sessions for Monkey T (***a***) and Monkey O (***b***). The two quantiles are the 15% largest (slowest) RTs and the 15% smallest (fastest) RTs. The power spectra have been normalized, and their *z* scores are plotted against frequency (Hertz). Gray represents SE over sessions. ***c***, Correlation between normalized poststimulus power spectra with RT as a function of frequency. Data were separately averaged for each monkey over electrodes. Next, data were combined for the 2 monkeys and were averaged over sessions. *Points along the curve where the correlation is significant (adjusted *p* value <0.05, sign test).

We repeated the same correlational analysis across all sessions and over all coherences. For each session, we computed the partial Spearman correlation between RT and BBA at each frequency while controlling for the coherence of the checkerboard. We then averaged the partial correlations over the electrodes for each session and then over sessions. Correlation analyses exploiting the simultaneous nature of our recordings were not notably different from the averaging analysis, so we only report the results obtained from averaging partial correlations over electrodes. Consistent with the analyses of peak frequency detailed above and the single example session, we found a positive correlation between BBA and RT ~15 Hz (at 15.625 Hz, $r = 0.04$ with $p = 2.59 \times 10^{-4}$) and a negative correlation between BBA and RT at ~30 Hz (at 31.25 Hz, $r = -0.05$ with $p = 0.03$; Fig. 4*d*).

These population analyses suggest that the presence of significant correlations is inconsistent with the postural holding hypothesis. However, varying correlations by frequency are consistent with both the maintenance hypothesis (purely positive correlations with BBA) and the attentional hypothesis (purely negative correlations with BBA) within different subregions of the beta band (maintenance for low BBA and attentional for high BBA).

RT covaries with poststimulus BBA power and frequency, and poststimulus γ band power

We next repeated these analyses on the poststimulus (postcheckerboard) BBA to better understand its relation to RT. Across both monkeys during the poststimulus period, the slower RTs (85th percentile) have more power in the lower frequencies of BBA (~15–25 Hz; Fig. 5*a*,*b*). In Monkey O, in the higher frequencies of BBA (~25 to 35 Hz), the faster RTs have more power. Combined, this leads to a frequency shift between the RT quantiles, with the power spectra for the slower RT trials slightly shifted toward the lower frequencies. In Monkey T, the slower RTs have more power for both the low and high frequencies of BBA, so the perceived shift is perhaps less apparent.

We again computed the peak frequency for the poststimulus BBA and found a significant increase in peak frequency for faster RTs (0.67 Hz higher median peak frequency for the faster RT trials, $p = 6.738 \times 10^{-5}$). Similarly, partial correlations between BBA peak frequency and RT were modest but significant (median $r = -0.011$ with $p = 0.029$). Finally, across both monkeys, the correlation between poststimulus power and RT is positive for both low and high beta (at 21.48 Hz, $r = 0.12$ with $p = 4.84 \times 10^{-20}$; Fig. 5*c*). We found for the poststimulus period that the correlation is negative for γ activity in the low γ band (at 46.88 Hz, $r = -0.04$, with $p = 3.6149 \times 10^{-5}$), which is consistent with the increase in low γ activity from the prestimulus to poststimulus periods seen in Figure 3*f*.

Our analysis thus far has revealed that multiple facets of prestimulus and poststimulus BBA (and to some extent γ band activity) covary with RT. To better understand the relationship between RT and prestimulus and poststimulus BBA power and frequency, we used each of these variables as regressors to a GLM that attempted to explain log RT as a linear mixture of the components. We used log RT instead of RT alone to make this analysis comparable with the Spearman rank correlation method we used for the correlation analyses. Specifically, we regressed log RT with the factors: coherence, prestimulus low beta power (10–20 Hz), prestimulus high beta power (21–29 Hz), poststimulus low beta power (10–20 Hz), poststimulus high beta power (21–29 Hz), prestimulus peak frequency of BBA, poststimulus peak frequency of BBA, and an intercept. We used linear regression to estimate the coefficients for each session and a sign test to test for significance.

The results closely followed the trends of the correlations we performed. Coherence (our experimental manipulation) was negatively related to RT ($b = -0.082$, $p = 3.09 \times 10^{-17}$). Prestimulus low beta power was positively related to RT ($b = 0.014$, $p = 0.049$), whereas prestimulus high beta power was negatively related to RT ($b = -0.0122$, $p = 6.74 \times 10^{-5}$). Prestimulus peak frequency of BBA was negatively related to RT ($b = -6.2 \times 10^{-4}$, $p = 0.049$), and poststimulus peak frequency of BBA was negatively related to RT ($b = -5.9 \times 10^{-4}$, $p = 0.007$). Finally, both poststimulus low and high beta power were also positively related to RT ($b = 0.019$ with $p = 2.17 \times 10^{-5}$ and $b = 0.017$ with $p = 1.02 \times 10^{-10}$, respectively).

Together, these different analyses suggest the following picture: for the prestimulus period, faster RTs are accompanied by a shift in the BBA toward the higher beta frequencies, whereas slower RTs are accompanied by lower beta frequencies. For the poststimulus period, the pattern is more nuanced; slower RTs are accompanied by across the board increases in beta band power, whereas faster RTs are accompanied by higher frequencies of BBA and by an increase in γ band activity.

One potential interpretation for our results for the poststimulus period is a shift in the component frequencies of the LFP, this time across multiple frequency bands, as well as an increase in

power in the γ band. That is, on faster RT trials, there could be less overall BBA and slightly more low γ band activity, with the opposite being true for the slower RTs.

Simulations further suggest that frequency shift in BBA as a plausible mechanism for the observed pattern of correlation

One concern from the analyses presented above is that the correlation and regression patterns we see in the BBA are somehow artifactual and are arising largely from the changes in power as a function of RT. We therefore performed a simple simulation to better understand the patterns of correlations between RT and power at each frequency. We do not propose that these simulations are in any way physiologically representative. Instead, the goal of these simulations is to reaffirm the patterns that we observed from analysis of the relationship between BBA and RT, and to ensure they are not an artifact of our correlation analyses.

The schematic for this simulation analysis is shown in Figure 6*a*. First, we randomly generated RT values within the range of RTs typically observed for our monkeys. Then, based on these values and a variety of governing equations for frequency and amplitude, we simulated LFP signals for these hypothetical trials. The signal was defined as follows:

$$signal = Amplitude * sin(2\pi * Frequency * t)$$

where amplitude and frequency are constants, linear increasing functions of RT, or linear decreasing functions of RT, with added noise. We then calculated the power spectra of these simulated signals from these trials and correlated these power spectra to their corresponding RTs. For each group of frequency and amplitude equations, we generated 1000 simulated trials with corresponding RTs, simulated LFP signals, and power spectra. The correlation coefficient as a function of frequency between the simulated power spectra and RTs is shown in Figure 6*b* for the six paradigms.

We first considered the simple case that power (amplitude) in BBA changes with RT. Power modulation alone fails to explain the observed correlation pattern shown in Figure 4*d* (in Fig. 6*bi–ii*). The correlations between prestimulus BBA and RT observed in the real data (shown in Fig. 4*d*) most closely match the correlation when frequency is negatively related to RT. This relationship is robust regardless of the relationship between amplitude and RT (shown in Fig. 6*biv–vi*). These findings indicate the presence of a relationship between prestimulus BBA frequency composition and RT, suggesting that prestimulus BBA component frequencies are negatively related with RT. We note that these simulations have only suggested one plausible mechanism, which is a change in the center frequency of the beta band. A change in proportions of bursts at low and high beta frequencies is another potential mechanism for explaining these results.

These simulations also suggest that when BBA frequency is negatively correlated with RT, the point at which correlations shift from positive to negative is modulated by the relationship between BBA power and RT. The correlations between poststimulus BBA and RT observed in the real data (shown in Fig. 5*c*) most closely match the correlation when BBA frequency is negatively related to RT and amplitude is positively related to RT (Fig. 6*bv*) because the switch from positive to negative correlations happens at a higher frequency when BBA amplitude is positively correlated with RT. These simulation results provide additional credence to our postulate that faster RTs are accompanied by higher frequencies of BBA both prestimulus and poststimulus.

Slower RT trials are accompanied by low beta activity before cue onset

Our analysis of BBA has thus far focused on the entirety of the prestimulus and poststimulus interval. However, it is increasingly clear from multiple studies that BBA is transient and perhaps, when averaged over multiple trials, appears to be sustained (Feingold et al., 2015; Lundqvist et al., 2016; Shin et al., 2017). The use of wavelets allows better time and frequency resolution in estimating how BBA varies across time. We therefore recomputed the time–frequency representation of our data, this time using Morlet wavelets (Fig. 7*a*). This wavelet analysis again confirms the presence of both low and high BBA in the 600 ms before the checkerboard cue. After the checkerboard cue appears, BBA decreases again.

To better understand how BBA relates to RT over the time course of the task, we computed the partial correlation of each voxel of the spectrograms with RT while controlling for stimulus coherence. After controlling for multiple comparisons using the FDR procedure ($p < 0.05$), we identified regions with significant correlations, with the rest set to zero (Fig. 7*b*). Well before the checkerboard onset (~−600 ms to −500 ms before), high BBA (~20–30 Hz), and low γ band activity are negatively correlated with RT. At the time of checkerboard onset, high BBA is negatively correlated with RT (−300 ms up to the appearance of the checkerboard) with low BBA positively correlated with RT. After the stimulus, the correlation becomes positive for both low and high BBA and negative for the γ band. These findings with the wavelet analyses are reassuringly consistent with our findings in Figures 4*d* and 5*c* for the overall prestimulus and poststimulus periods.

Some studies have investigated the temporal relationship between BBA and behavior (Shin et al., 2017). To better understand the relationship between temporal profile of BBA and RT, we again split the trials into those with the 15% slowest (largest) RTs and the 15% fastest (smallest) RTs. After averaging the spectrograms over trials and then electrodes, we found the difference between the two (spectrogram for slowest, fastest) and then averaged over sessions. After controlling the FDR using the FDR procedure, we plotted spectrogram values with significant differences (Fig. 7*c*; $p < 0.05$). We also averaged the difference spectrogram from Figure 7*c* over 200 ms time bins and plotted the difference power spectra and the error over sessions in Figure 7*d*.

Well before the checkerboard onset (~600–400 ms before, Fig. 7*c*,*d*), the presence of high beta activity is greater in trials with fast RTs than those with slow RTs. This suggests that greater high beta activity well before the checkerboard onset is associated with smaller RTs. These results are overall consistent with our correlational analysis of the entire prestimulus period (from 600 ms before checkerboard onset to the appearance of the checkerboard), which suggested that high beta was negatively correlated with RT (Fig. 4*d*).

Close to the appearance of the checkerboard (from 200 ms before to checkerboard onset), the presence of low beta activity is greater in trials with slow RTs than those with fast RTs. Thus, greater low beta activity immediately before the checkerboard appears to be associated with larger RTs, a result broadly consistent with findings that beta events before stimulus onset have a deleterious impact on perception (Shin et al., 2017).

After the appearance of the checkerboard but largely before movement onset (up to ~200 ms after), the presence of both low and high beta activity is greater in trials with slow RTs than those with fast RTs, which is consistent with our correlational findings for the overall poststimulus period (Fig. 5*c*).

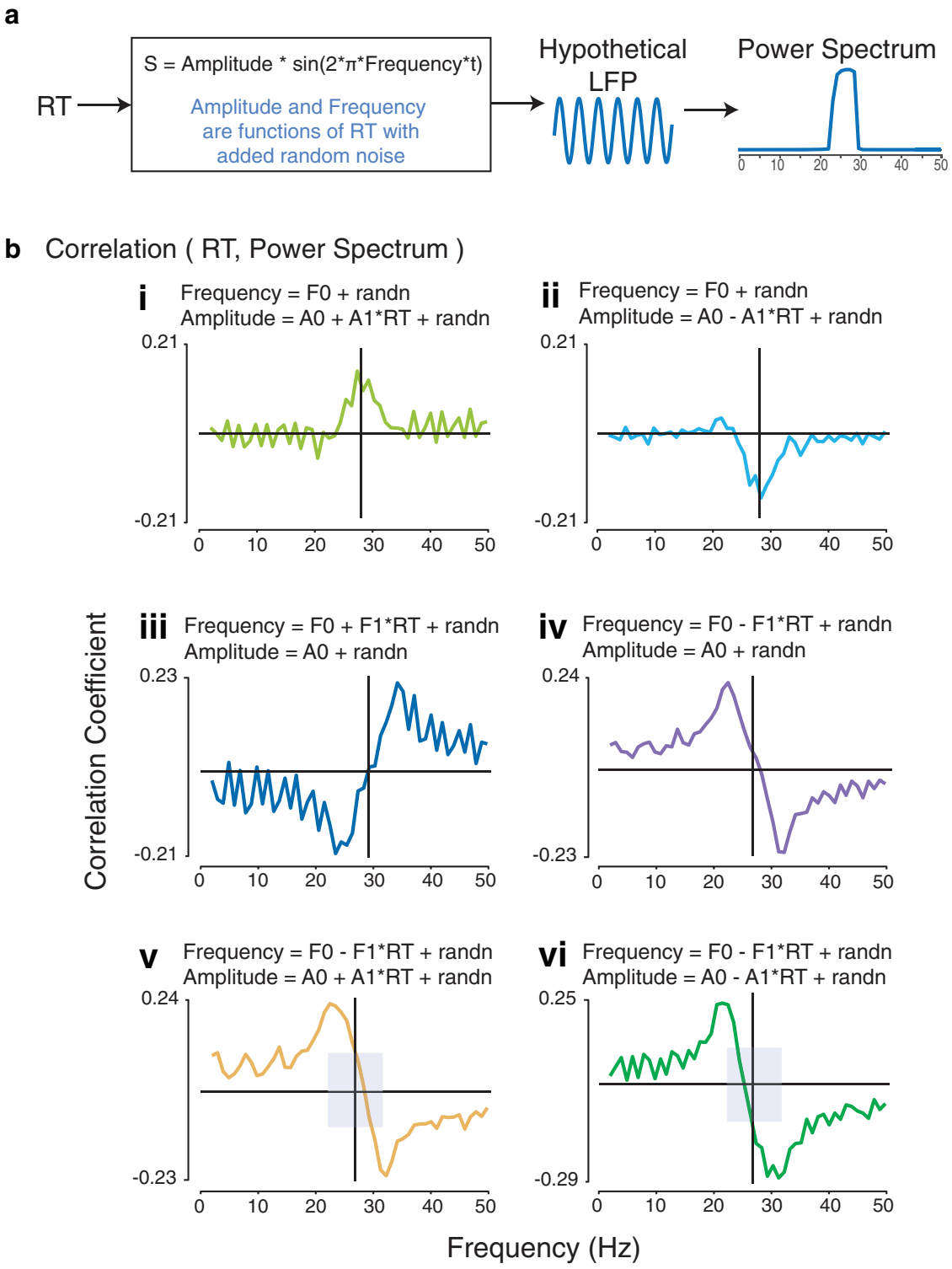

Figure 6. Simulations of relation between BBA and RT. Process (***a***) and results (***b***) of a simulation that generated synthetic LFP signals as Amplitude * sin(2 * π * Frequency * *t*). The amplitude and frequency of the LFP were defined differently for each case, either as a constant or a function of RT. In all cases, random noise was added to these variables. Power spectra were made from these LFP signals, and they were then correlated with RT to create the shown plots of correlation coefficients as a function of frequency for each of the six cases. The amplitude and frequency relationships with RT for each case are shown with the correlations.

Deeper cortical layers have stronger activity in the low beta range than the superficial layers

The secondary goal of our study was to further clarify how BBA changes as a function of cortical depth. The use of linear multicontact electrodes (Fig. 2*g*) provided us with simultaneous recordings across several cortical depths and allowed us to examine whether there was a relationship between cortical depth and BBA.

To examine the degree to which prestimulus power in the beta region varied with electrode depth, we divided the electrodes into two groups: the superficial (electrodes 1:8) and the deep (elec-

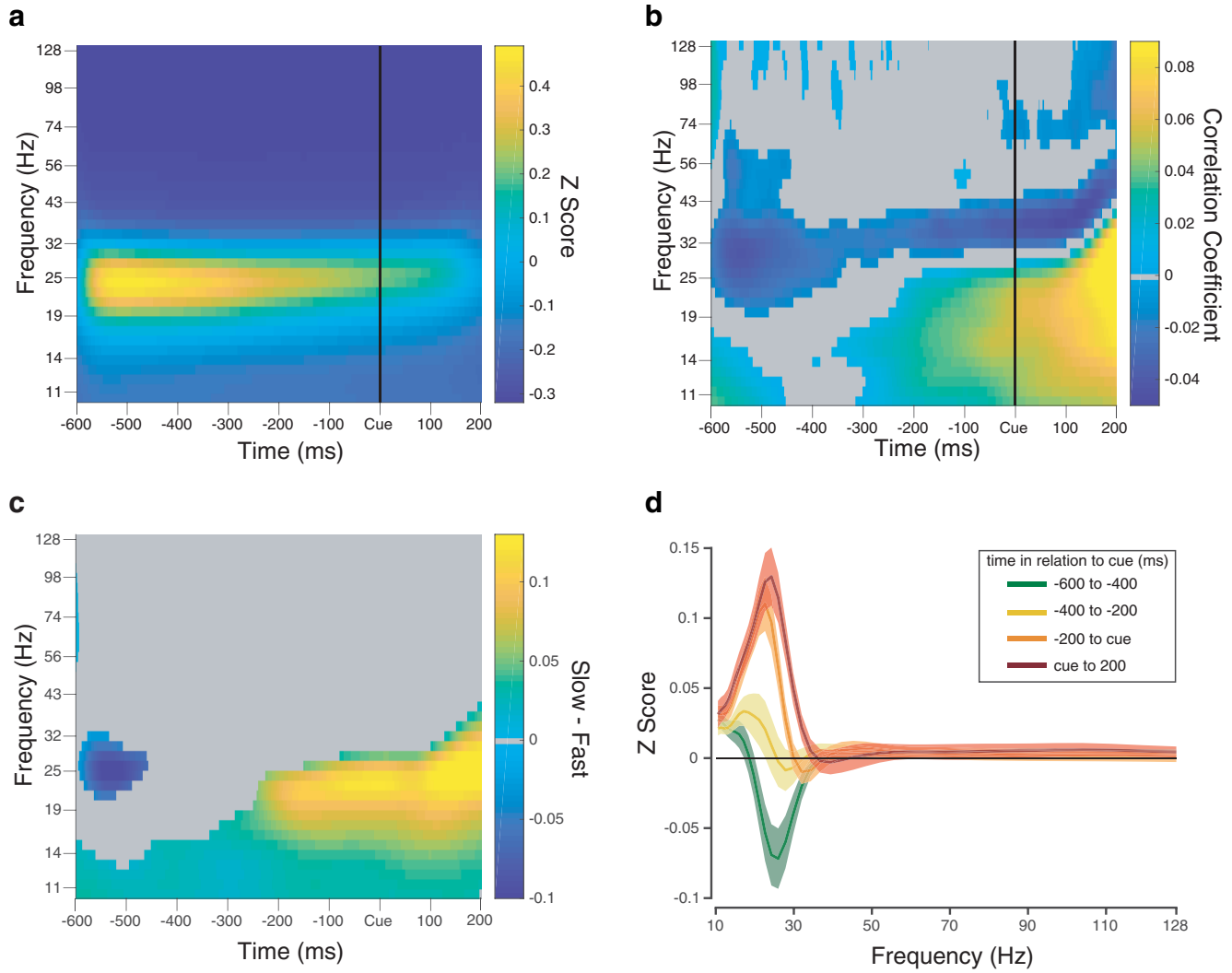

Figure 7. Wavelets help resolve the time modulation of BBA. ***a***, Spectrogram computed using Morelet wavelets averaged over trials, electrodes, and sessions. *x* axis represents time in milliseconds; *y* axis represents the frequency in Hertz. Warmer (yellower) colors represent higher power. ***b***, Partial correlation between each voxel of the Morelet wavelet spectrogram and RT, controlling for checkerboard coherence. Gray represents nonsignificant correlations (after FDR corrections), which were set to zero. ***c***, Spectrogram difference between the 15% slowest (largest) RTs and 15% fastest (smallest) RTs. The spectrograms were averaged over trials and electrodes before the spectrogram for the fastest RTs was subtracted from that of the slowest RTs, and then the difference spectrogram was averaged over sessions. Gray represents points for which the *t* test was not significant (after FDR corrections), which were set to zero. ***d***, Power spectra of difference between the 15% slowest (largest) RTs and 15% fastest (smallest) RTs for different 200 ms time periods. Spectrograms were averaged over trials and electrodes before the spectrogram for the fastest RTs was subtracted from that of the slowest RTs; then this was averaged over 200 ms time bins and then averaged over sessions. Shading represents SE over sessions.

trodes 9:16). Deeper electrodes (coarsely corresponding to deeper cortical layers) have more power at the ~10–20 Hz region (Fig. 8*a*; median power difference of 0.067, distributions across sessions significantly different with $p = 6.80 \times 10^{-16}$). The peak frequency is also different for superficial and deep electrodes. The peak frequency for superficial electrodes is also higher than that of deep electrodes (median difference of 0.95 Hz, distributions significantly different with $p = 1.49 \times 10^{-12}$).

This pattern of deeper electrodes having more power than surface electrodes at the ~10–20 Hz (low beta) region is also true of the poststimulus period (Fig. 8*c*; median power difference of 0.031, distributions across sessions significantly different with $p = 4.0421 \times 10^{-9}$). During the poststimulus period, the peak frequency for superficial electrodes is higher than that of deep electrodes (median difference of 0.56 Hz, distributions significantly different with $p = 4.04 \times 10^{-9}$).

These results both prestimulus and poststimulus are consistent with a recent report that examined LFPs in rostral PMd and found higher levels of alpha and BBA in deeper layers of cortex, whereas γ was more prevalent in the superficial layers of cortex (Bastos et al., 2018).

Correlation between BBA and RT does not vary significantly by depth

To examine whether BBA from certain cortical layers was more strongly tied with RTs, we performed the partial correlation with RT over two depth groups: superficial (electrodes 1:8) and deep (electrodes 9:16). For both prestimulus (Fig. 8*b*) and poststimulus BBA (Fig. 8*d*), the correlations for each group of electrodes produced the same shape as the correlation over all electrodes shown previously. The correlations for the superficial and deep electrodes are essentially the same, the correlation for one depth group is not dramatically different in magnitude or shape than that of the other. In the previous section, we showed that the peak frequencies for BBA were different at the level of the power spectra. However, the frequencies at which the correlation peaked

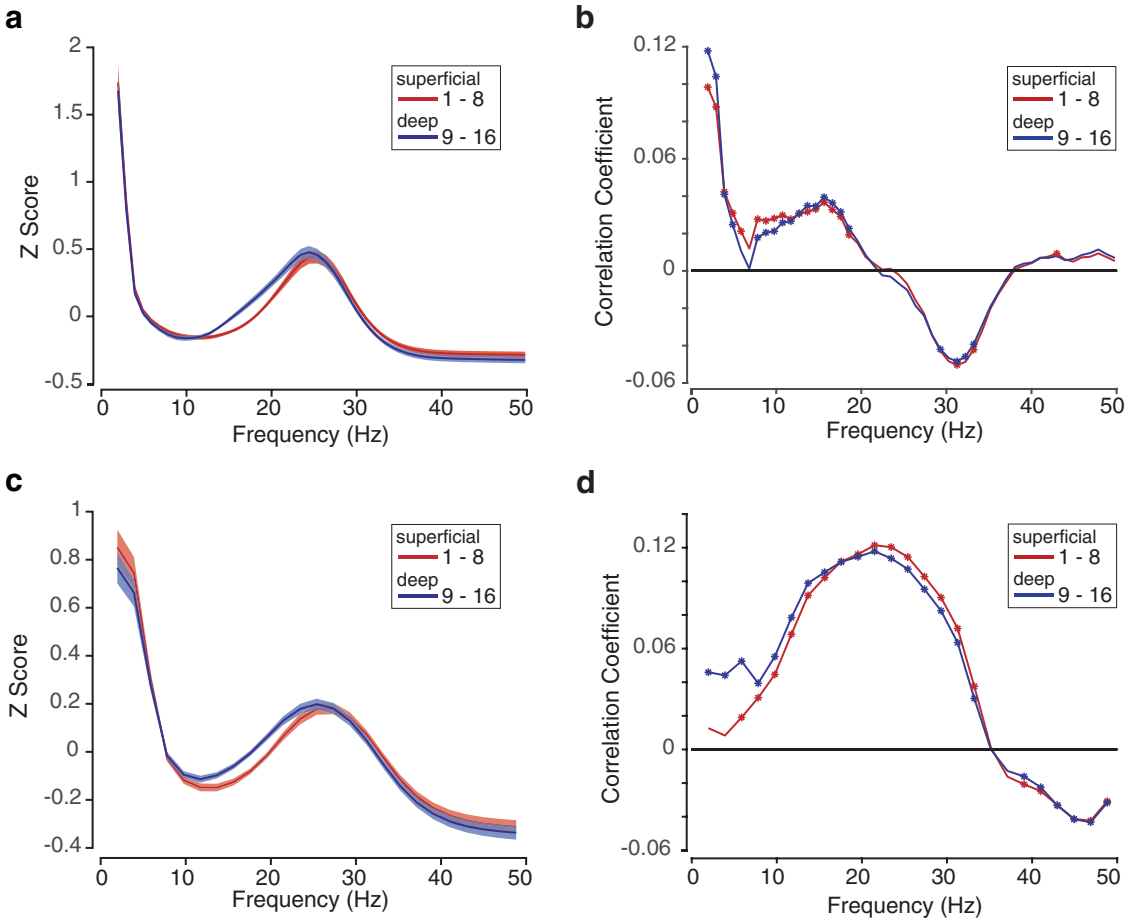

Figure 8. Prestimulus and poststimulus BBA by depth. ***a***, Normalized prestimulus power spectra grouped into two electrode groupings and averaged over all trials, all electrodes within that group, and all sessions for Monkey T and Monkey O. The power spectra have been normalized, and their *z* scores are plotted against frequency (Hertz). Red represents the average over the superficial electrodes. Blue represents the average over the deep electrodes. Shading represents SE over sessions. ***b***, Depth-dependent correlation between normalized prestimulus power spectra with RT as a function of frequency. Data were separately averaged for each monkey over trials and then separately for each depth group over electrodes. Next, data for each group were combined for the 2 monkeys and were averaged over sessions. Red represents the correlation over the superficial electrodes. Blue represents the correlation over the deep electrodes. ***c***, Normalized poststimulus power spectra grouped into two electrode groupings and averaged over all trials, all electrodes within that group, and all sessions combined across both monkeys. The power spectra have been normalized, and their *z* scores are plotted against frequency (Hertz). Red represents the average over the superficial electrodes. Blue represents the average over the deep electrodes. Shading represents SE. ***d***, Depth-dependent correlation between normalized poststimulus power spectra with RT as a function of frequency over both monkeys. Red represents the correlation over the superficial electrodes. Blue represents the correlation over the deep electrodes.

were also not significantly different between superficial and deep electrodes during either period; during the prestimulus period, deep peaks at a slightly higher median frequency by 0.49 Hz, $p = 0.58$; and during the poststimulus period, superficial peaks at a higher median frequency by 0.98 Hz, $p = 0.32$).

Discussion

The motivation for our study was to further understand the behavioral relevance of BBA and how it is organized as a function of cortical depth. In a perceptual decision-making task, we found that BBA was robustly present during the prestimulus and poststimulus periods and was related to the behavioral RT. During the prestimulus period, low beta frequencies (~15–20 Hz) were positively correlated with RT, whereas high beta frequencies (~25–30 Hz) were negatively correlated. The observed frequency-dependent correlation might correspond to a negative relationship between RT and the component frequencies of prestimulus BBA. During the poststimulus period, all frequencies of BBA (~15–35 Hz) were positively correlated to RT. We also found that deeper electrodes had higher power in the low beta frequencies (~15–20 Hz) than superficial electrodes for both the prestimulus and poststimulus periods.

"Maintenance of current state" and "attentional" hypotheses help explain BBA in PMd

The nuanced relationship we discovered between BBA and RT is relevant for the ongoing discussion regarding the role of BBA. Currently, three main hypotheses exist, and each hypothesis has corresponding expected relationships between BBA and RT.

The postural hypothesis posits that BBA is a result of the maintained holding of a hand position and has no relationship to eventual behavior. For our experiment, one would predict no relationship between BBA and RT (Baker et al., 1999; Kristeva et al., 2007), a hypothesis inconsistent with our findings that both prestimulus and poststimulus BBA were related to RT.

Correlations between BBA and RT during the prestimulus period support both of the two remaining hypotheses. The maintenance hypothesis asserts that BBA represents a willingness to maintain the current state of either rest or movement, with greater levels of BBA reflecting the "desire" to maintain the hold

position and resulting in slower movement and an increase in RT (Gilbertson et al., 2005; Pogosyan et al., 2009; Engel and Fries, 2010). Our finding of a positive correlation between BBA and RT for low beta frequencies is consistent with the maintenance hypothesis. The attentional hypothesis, which suggests that greater BBA reflects more attentional engagement with the task, would suggest a negative correlation between BBA and RT (Bouyer et al., 1987; Murthy and Fetz, 1992; Zhang et al., 2008; Saleh et al., 2010). The negative correlation between BBA and RT for high beta frequencies supports the attentional hypothesis.

During the poststimulus period, we found that BBA was positively correlated with RT for both low and high frequencies, which is consistent with the maintenance hypothesis. During this period, it appears as if BBA of any frequency (low or high) reflects processes incompatible with movement initiation, such as a willingness to maintain the current state of being.

This constellation of results suggests that the beta band is not a monolithic signal and consists of activity in at least two frequency sub-bands that dynamically emerge in different task epochs, perhaps reflecting distinct behavioral demands placed on the animal (Buschman et al., 2012; Spitzer and Haegens, 2017). We expand on this theme in the next section.

BBA is better understood when split into two frequency bands

By examining the correlation at each frequency, rather than averaging over the whole beta frequency band, we found that BBA is better understood as being composed of at least two frequency sub-bands: low beta (~13–20 Hz) and high beta (~25–30 Hz). Future work should test whether there are distinct beta1 and beta2 bursts or just modulation of the dominant frequency of BBA (Lundqvist et al., 2016; Shin et al., 2017).

Our nuanced view of BBA has some precedent in literature, with human EEG, rat studies, and some monkey studies referring to a beta1 band (~15 Hz) and a beta2 band (~25 Hz) (Haenschel et al., 2000; Kramer et al., 2008; Khayat et al., 2010; Kopell et al., 2011; Cannon et al., 2014). In monkeys, Kilavik et al. (2012) examined motor cortical BBA during a visual multiple delay reaching task and suggested a similar separation. They posited that low beta frequencies were the result of widespread networks involved in top-down (conscious) processing and expectation of movement-related visual information, whereas higher beta frequencies emerged from bottom-up visual information processing and movement preparation (Kilavik et al., 2012).

The prestimulus period of our task incorporates the behavioral components identified by Kilavik et al. (2012) for both frequency sub-bands of BBA - the monkey is expecting the visual checkerboard stimulus, is viewing relevant reach targets, and is preparing for one of two arm movements. We take the stance that the frequency composition of the prestimulus period reflects these different processes in the decision-making task. Therefore, it is not unreasonable that we see both low and high beta frequencies and positive and negative correlations between BBA and RT.

As the task progresses, the visual checkerboard (a bottom-up visual stimulus) appears. We speculate that the appearance of the checkerboard triggers a cognitive process that involves deliberation on the visual stimulus and likely movement preparation for the arm movement to report the decision. In the framework proposed by Kilavik and collaborators, such processes should induce activity in multiple beta frequencies, which is consistent with the broader frequency range of BBA and γ band activity we see in the poststimulus period. It remains to be understood why increased beta of any frequency during this period is associated with slower RTs.

Beyond the LFP

Our study has focused on BBA in the LFP and behavior. We chose to analyze the LFP because it provides a population-level, spatially averaged description of neural activity. We anticipate similar effects in spiking neurons, and preliminary analysis of our spike trains suggested BBA in many neurons and multiunits. However, analysis of single-neuron spike trains is often difficult because of the mixture of both Poisson and non-Poisson variability in these spike trains. Typical noise-reduction steps, such as convolution of spike trains with various filters, end up low pass filtering spike trains, which would lead to severe attenuation of signals at beta frequencies and the overemphasis of slower dynamics. We take the view that these spikes and LFPs are emerging from a dynamical system with activity at multiple time scales and that there is a need for collectively understanding both slow and fast dynamics in neural activity. Single-trial analysis methods, including those that use recurrent neural networks, would facilitate such analyses (Pandarinath et al., 2018).

Greater low-frequency beta in deeper electrodes is consistent with hypotheses about the generation of BBA

We found that electrodes placed deeper in the cortex, whose position approximately corresponds to layer V, have higher power in the low beta range (~15–20 Hz) than superficially placed electrodes during both the prestimulus and poststimulus periods.

Two main hypotheses exist regarding the generation of BBA: it is either generated locally, perhaps in layer V of motor cortex, or it is generated distally and transmitted from elsewhere (Khanna and Carmena, 2015; Spitzer and Haegens, 2017). Our finding of greater power in low beta frequencies for deeper electrodes is consistent with both predominant hypotheses; greater power could either indicate the BBA being generated in that layer (local hypothesis), or it could indicate that the distally generated BBA is projected into that layer (distal hypothesis).

A few studies have examined relationships between BBA and cortical depth. One study examined synchronization of BBA at various depths in the inferior temporal cortex during the passive repetition of visual stimuli (Kaliukhovich and Vogels, 2012). A recent laminar study of LFP power in frontal cortex, including rostral PMd, found greater power for low frequencies of BBA in deeper cortical layers (Bastos et al., 2018) - a result that predicted our observations here. In the future, we expect it to be possible to combine methods that estimated the current source density using flashed wide-field stimuli (Godlove et al., 2014; Bastos et al., 2018) with the power and correlation analyses presented here to better understand how BBA changes across cortical layers during decision-making.

Even though few studies focus on how BBA changes as a function of cortical depth, many have hypothesized about its origin and built computational models (Lee et al., 2013; Cannon et al., 2014). Despite these studies advancing our understanding of the biophysical basis of BBA, we still lack clarity about its underlying generators because these modeling studies focus on results from *in vitro* experiments in sensory cortices, with only one study focusing on the motor areas. Our study complements Bastos et al. (2018) and provides further evidence from premotor cortical areas in monkeys performing demanding cognitive tasks that also involve the somatomotor system. We anticipate that our data showing greater power in the lower frequencies of BBA will help constrain computational models of BBA. Studies involving lam-

inar recordings in other BBA-associated structures are needed to build the next generation of computational models of BBA. Ideally, these future studies would include decision-making, instructed delay, and somatosensory perturbation tasks that engage the different processes that are postulated to be associated with BBA.

References

Bai O, Lin P, Vorbach S, Floeter MK, Hattori N, Hallett M (2008) A high performance sensorimotor beta rhythm-based brain-computer interface associated with human natural motor behavior. J Neural Eng 5:24–35. CrossRef Medline

Baker SN (2007) Oscillatory interactions between sensorimotor cortex and the periphery. Curr Opin Neurobiol 17:649–655. CrossRef Medline

Baker SN, Olivier E, Lemon RN (1997) Coherent oscillations in monkey motor cortex and hand muscle EMG show task-dependent modulation. J Physiol 501:225–241. CrossRef Medline

Baker SN, Kilner JM, Pinches EM, Lemon RN (1999) The role of synchrony and oscillations in the motor output. Exp Brain Res 128:109–117. CrossRef Medline

Bastos AM, Loonis R, Kornblith S, Lundqvist M, Miller EK (2018) Laminar recordings in frontal cortex suggest distinct layers for maintenance and control of working memory. Proc Natl Acad Sci U S A 115:1117–1122. CrossRef Medline

Benjamini Y, Hochberg Y (1995) Controlling the false discovery rate: a practical and powerful approach to multiple testing. J R Stat Soc Series B Stat Methodol 57:289–300.

Bhatt MB, Bowen S, Rossiter HE, Dupont-Hadwen J, Moran RJ, Friston KJ, Ward NS (2016) Computational modelling of movement-related beta-oscillatory dynamics in human motor cortex. Neuroimage 133:224–232. CrossRef Medline

Bouyer JJ, Montaron MF, Vahnée JM, Albert MP, Rougeul A (1987) Anatomical localization of cortical beta rhythms in cat. Neuroscience 22:863–869. CrossRef Medline

Brittain JS, Sharott A, Brown P (2014) The highs and lows of beta activity in cortico-basal ganglia loops. Eur J Neurosci 39:1951–1959. CrossRef Medline

Brown P (2006) Bad oscillations in Parkinson's disease. J Neural Transm Suppl 70:27–30. CrossRef Medline

Buschman TJ, Miller EK (2007) Top-down versus bottom-up control of attention in the prefrontal and posterior parietal cortices. Science 315:1860–1862. CrossRef Medline

Buschman TJ, Denovellis EL, Diogo C, Bullock D, Miller EK (2012) Synchronous oscillatory neural ensembles for rules in the prefrontal cortex. Neuron 76:838–846. CrossRef Medline

Cannon J, McCarthy MM, Lee S, Lee J, Börgers C, Whittington MA, Kopell N (2014) Neurosystems: brain rhythms and cognitive processing. Eur J Neurosci 39:705–719. CrossRef Medline

Chakarov V, Naranjo JR, Schulte-Mönting J, Omlor W, Huethe F, Kristeva R (2009) Beta-range EEG-EMG coherence with isometric compensation for increasing modulated low-level forces. J Neurophysiol 102:1115–1120. CrossRef Medline

Chandrasekaran C, Ghazanfar AA (2009) Different neural frequency bands integrate faces and voices differently in the superior temporal sulcus. J Neurophysiol 101:773–788. CrossRef Medline

Chandrasekaran C, Peixoto D, Newsome WT, Shenoy KV (2017) Laminar differences in decision-related neural activity in dorsal premotor cortex. Nat Commun 8:614. CrossRef Medline

Chen D, Fetz EE (2005) Characteristic membrane potential trajectories in primate sensorimotor cortex neurons recorded in vivo. J Neurophysiol 94:2713–2725. CrossRef Medline

Coallier E, Michelet T, Kalaska JF (2015) Dorsal premotor cortex: neural correlates of reach target decisions based on a color-location matching rule and conflicting sensory evidence. J Neurophysiol 113:3543–3573. CrossRef Medline

Computational Memory Lab of University of Pennsylvania (2008) EEG Toolbox. Available at http://memory.psych.upenn.edu/files/software/eeg_toolbox/eeg_toolbox.zip.

Cooper GF, Robson JG, Waldron I (1969) The action potentials recorded from undamaged nerve fibres with micro-electrodes. J Physiol 200:9P–11P. Medline

Engel AK, Fries P (2010) Beta-band oscillations-signalling the status quo? Curr Opin Neurobiol 20:156–165. CrossRef Medline

Feingold J, Gibson DJ, DePasquale B, Graybiel AM (2015) Bursts of beta oscillation differentiate postperformance activity in the striatum and motor cortex of monkeys performing movement tasks. Proc Natl Acad Sci U S A 112:13687–13692. CrossRef Medline

Flint RD, Wright ZA, Scheid MR, Slutzky MW (2013) Long term, stable brain machine interface performance using local field potentials and multiunit spikes. J Neural Eng 10:056005. CrossRef Medline

Ghazanfar AA, Chandrasekaran C, Logothetis NK (2008) Interactions between the superior temporal sulcus and auditory cortex mediate dynamic face/voice integration in rhesus monkeys. J Neurosci 28:4457–4469. CrossRef Medline

Gilbertson T, Lalo E, Doyle L, Di Lazzaro V, Cioni B, Brown P (2005) Existing motor state is favored at the expense of new movement during 13–35 Hz oscillatory synchrony in the human corticospinal system. J Neurosci 25:7771–7779. CrossRef Medline

Gilja V, Pandarinath C, Blabe CH, Nuyujukian P, Simeral JD, Sarma AA, Sorice BL, Perge JA, Jarosiewicz B, Hochberg LR, Shenoy KV, Henderson JM (2015) Clinical translation of a high-performance neural prosthesis. Nat Med 21:1142–1145. CrossRef Medline

Godlove DC, Maier A, Woodman GF, Schall JD (2014) Microcircuitry of agranular frontal cortex: testing the generality of the canonical cortical microcircuit. J Neurosci 34:5355–5369. CrossRef Medline

Groppe D (2015) fdr_bh. Available at https://www.mathworks.com/matlabcentral/fileexchange/27418-fdr_bh.

Haegens S, Vergara J, Rossi-Pool R, Lemus L, Romo R (2017) Beta oscillations reflect supramodal information during perceptual judgment. Proc Natl Acad Sci U S A 114:13810–13815. CrossRef Medline

Haenschel C, Baldeweg T, Croft RJ, Whittington M, Gruzelier J (2000) Gamma and beta frequency oscillations in response to novel auditory stimuli: a comparison of human electroencephalogram (EEG) data with in vitro models. Proc Natl Acad Sci U S A 97:7645–7650. CrossRef Medline

Kaliukhovich DA, Vogels R (2012) Stimulus repetition affects both strength and synchrony of macaque inferior temporal cortical activity. J Neurophysiol 107:3509–3527. CrossRef Medline

Keitel A, Gross J (2016) Individual human brain areas can be identified from their characteristic spectral activation fingerprints. PLoS Biol 14:e1002498. CrossRef Medline

Khanna P, Carmena JM (2015) Neural oscillations: beta band activity across motor networks. Curr Opin Neurobiol 32:60–67. CrossRef Medline

Khanna P, Carmena JM (2017) Beta band oscillations in motor cortex reflect neural population signals that delay movement onset. Elife 6:e24573. CrossRef Medline

Khayat PS, Niebergall R, Martinez-Trujillo JC (2010) Frequency-dependent attentional modulation of local field potential signals in macaque area MT. J Neurosci 30:7037–7048. CrossRef Medline

Kilavik BE, Ponce-Alvarez A, Trachel R, Confais J, Takerkart S, Riehle A (2012) Context-related frequency modulations of macaque motor cortical LFP beta oscillations. Cereb Cortex 22:2148–2159. CrossRef Medline

Kilavik BE, Zaepffel M, Brovelli A, MacKay WA, Riehle A (2013) The ups and downs of β oscillations in sensorimotor cortex. Exp Neurol 245:15–26. CrossRef Medline

Kilner JM, Baker SN, Salenius S, Jousmäki V, Hari R, Lemon RN (1999) Task-dependent modulation of 15–30 Hz coherence between rectified EMGs from human hand and forearm muscles. J Physiol 516:559–570. CrossRef Medline

Klostermann F, Nikulin VV, Kühn AA, Marzinzik F, Wahl M, Pogosyan A, Kupsch A, Schneider GH, Brown P, Curio G (2007) Task-related differential dynamics of EEG alpha- and beta-band synchronization in cortico-basal motor structures. Eur J Neurosci 25:1604–1615. CrossRef Medline

Kondabolu K, Roberts EA, Bucklin M, McCarthy MM, Kopell N, Han X (2016) Striatal cholinergic interneurons generate beta and gamma oscillations in the corticostriatal circuit and produce motor deficits. Proc Natl Acad Sci U S A 113:E3159–E3168. CrossRef Medline

Kopell N, Whittington MA, Kramer MA (2011) Neuronal assembly dynamics in the beta1 frequency range permits short-term memory. Proc Natl Acad Sci U S A 108:3779–3784. CrossRef Medline

Kramer MA, Roopun AK, Carracedo LM, Traub RD, Whittington MA, Kopell NJ (2008) Rhythm generation through period concatenation in rat somatosensory cortex. PLoS Comput Biol 4:e1000169. CrossRef Medline

Kristeva R, Patino L, Omlor W (2007) Beta-range cortical motor spectral power and corticomuscular coherence as a mechanism for effective corticospinal interaction during steady-state motor output. Neuroimage 36:785–792. CrossRef Medline

Lakatos P, Chen CM, O'Connell MN, Mills A, Schroeder CE (2007) Neuronal oscillations and multisensory interaction in primary auditory cortex. Neuron 53:279–292. CrossRef Medline

Lee D (2003) Coherent oscillations in neuronal activity of the supplementary motor area during a visuomotor task. J Neurosci 23:6798–6809. CrossRef Medline

Lee JH, Whittington MA, Kopell NJ (2013) Top-down beta rhythms support selective attention via interlaminar interaction: a model. PLoS Comput Biol 9:e1003164. CrossRef Medline

Lundqvist M, Rose J, Herman P, Brincat SL, Buschman TJ, Miller EK (2016) Gamma and beta bursts underlie working memory. Neuron 90:152–164. CrossRef Medline

Markowitz DA, Curtis CE, Pesaran B (2015) Multiple component networks support working memory in prefrontal cortex. Proc Natl Acad Sci U S A 112:11084–11089. CrossRef Medline

Mitra PP, Bokil H (2008) Observed brain dynamics. Oxford: Oxford UP.

Mitra P, Bokil H, Maniar H, Loader C, Mehta S, Hill D, Mitra S, Andrews P, Baptista R, Gopinath S, Nalatore H, Kaur S (2017) Chronux. Available at http://chronux.org/.

Murthy VN, Fetz EE (1992) Coherent 25- to 35-Hz oscillations in the sensorimotor cortex of awake behaving monkeys. Proc Natl Acad Sci U S A 89:5670–5674. CrossRef Medline

Pandarinath C, Nuyujukian P, Blabe CH, Sorice BL, Saab J, Willett FR, Hochberg LR, Shenoy KV, Henderson JM (2017) High performance communication by people with paralysis using an intracortical brain-computer interface. Elife 6:e18554. CrossRef Medline

Pandarinath C, O'Shea DJ, Collins J, Jozefowicz R, Stavisky SD, Kao JC, Trautmann EM, Kaufman MT, Ryu SI, Hochberg LR, Henderson JM, Shenoy KV, Abbott LF, Sussillo D (2018) Inferring single-trial neural population dynamics using sequential auto-encoders. Nat Methods 15:805–815. CrossRef Medline

Pesaran B, Nelson MJ, Andersen RA (2008) Free choice activates a decision circuit between frontal and parietal cortex. Nature 453:406–409. CrossRef Medline

Pogosyan A, Gaynor LD, Eusebio A, Brown P (2009) Boosting cortical activity at beta-band frequencies slows movement in humans. Curr Biol 19:1637–1641. CrossRef Medline

Proudfoot M, Rohenkohl G, Quinn A, Colclough GL, Wuu J, Talbot K, Woolrich MW, Benatar M, Nobre AC, Turner MR (2017) Altered cortical beta-band oscillations reflect motor system degeneration in amyotrophic lateral sclerosis. Hum Brain Mapp 38:237–254. CrossRef Medline

Riddle CN, Baker SN (2006) Digit displacement, not object compliance, underlies task dependent modulations in human corticomuscular coherence. Neuroimage 33:618–627. CrossRef Medline

Roitman JD, Shadlen MN (2002) Response of neurons in the lateral intraparietal area during a combined visual discrimination reaction time task. J Neurosci 22:9475–9489. CrossRef Medline

Roopun AK, Middleton SJ, Cunningham MO, LeBeau FE, Bibbig A, Whittington MA, Traub RD (2006) A beta2-frequency (20–30 Hz) oscillation in nonsynaptic networks of somatosensory cortex. Proc Natl Acad Sci U S A 103:15646–15650. CrossRef Medline

Rossiter HE, Davis EM, Clark EV, Boudrias MH, Ward NS (2014) Beta oscillations reflect changes in motor cortex inhibition in healthy ageing. Neuroimage 91:360–365. CrossRef Medline

Rubino D, Robbins KA, Hatsopoulos NG (2006) Propagating waves mediate information transfer in the motor cortex. Nat Neurosci 9:1549–1557. CrossRef Medline

Saleh M, Reimer J, Penn R, Ojakangas CL, Hatsopoulos NG (2010) Fast and slow oscillations in human primary motor cortex predict oncoming behaviorally relevant cues. Neuron 65:461–471. CrossRef Medline

Sanes JN, Donoghue JP (1993) Oscillations in local field potentials of the primate motor cortex during voluntary movement. Proc Natl Acad Sci U S A 90:4470–4474. CrossRef Medline

Sherman MA, Lee S, Law R, Haegens S, Thorn CA, Hämäläinen MS, Moore CI, Jones SR (2016) Neural mechanisms of transient neocortical beta rhythms: converging evidence from humans, computational modeling, monkeys, and mice. Proc Natl Acad Sci U S A 113:E4885–E4894. CrossRef Medline

Shin H, Law R, Tsutsui S, Moore CI, Jones SR (2017) The rate of transient beta frequency events predicts behavior across tasks and species. Elife 6:e29086. CrossRef Medline

So K, Dangi S, Orsborn AL, Gastpar MC, Carmena JM (2014) Subject-specific modulation of local field potential spectral power during brain–machine interface control in primates. J Neural Eng 11:026002. CrossRef Medline

Spitzer B, Haegens S (2017) Beyond the status quo: a role for beta oscillations in endogenous content (re)activation. eNeuro 4:ENEURO.0170–17.2017. CrossRef Medline

Stavisky SD, Kao JC, Nuyujukian P, Ryu SI, Shenoy KV (2015) A high performing brain–machine interface driven by low-frequency local field potentials alone and together with spikes. J Neural Eng 12:036009. CrossRef Medline

Stetson C, Andersen RA (2014) The parietal reach region selectively anti-synchronizes with dorsal premotor cortex during planning. J Neurosci 34:11948–11958. CrossRef Medline

Tallon-Baudry C, Bertrand O, Delpuech C, Permier J (1997) Oscillatory γ-band (30–70 Hz) activity induced by a visual search task in humans. J Neurosci 17:722–734. CrossRef Medline

Thura D, Cisek P (2014) Deliberation and commitment in the premotor and primary motor cortex during dynamic decision making. Neuron 81:1401–1416. CrossRef Medline

Tzagarakis C, Ince NF, Leuthold AC, Pellizzer G (2010) Beta-band activity during motor planning reflects response uncertainty. J Neurosci 30:11270–11277. CrossRef Medline

Wetmore DZ, Baker SN (2004) Post-spike distance-to-threshold trajectories of neurones in monkey motor cortex. J Physiol 555:831–850. CrossRef Medline

Wichmann FA, Hill NJ (2001) The psychometric function: I. Fitting, sampling, and goodness of fit. Percept Psychophys 63:1293–1313. CrossRef Medline

Yamawaki N, Stanford IM, Hall SD, Woodhall GL (2008) Pharmacologically induced and stimulus evoked rhythmic neuronal oscillatory activity in the primary motor cortex in vitro. Neuroscience 151:386–395. CrossRef Medline

Zaepffel M, Trachel R, Kilavik BE, Brochier T (2013) Modulations of EEG beta power during planning and execution of grasping movements. PLoS One 8:e60060. CrossRef Medline

Zhang Y, Wang X, Bressler SL, Chen Y, Ding M (2008) Prestimulus cortical activity is correlated with speed of visuomotor processing. J Cogn Neurosci 20:1915–1925. CrossRef Medline